END
DATE
FILMED
10-81
DTIC

MERCURY BROMIDE LASER RESEARCH

J. L. Pack, C. S. Liu, D. W. Feldman
and I. Liberman

May 4, 1981

LEVEL II

Period between July 1, 1980 and
March 31, 1981

Final Report

Contract No. N00014-80-C-0604 NEW

Office of Naval Research
800 North Quincy Street
Arlington, VA 22217

DTIC
SELECTED
SEP 0 3 1981
E

Westinghouse R&D Center
1310 Beulah Road
Pittsburgh, Pennsylvania 15235

MERCURY BROMIDE LASER RESEARCH

J. L. Pack, C. S. Liu, D. W. Feldman
and I. Liberman

May 4, 1981

Period between July 1, 1980 and
March 31, 1981

Final Report.

Contract No. N00014-80-C-0604

Office of Naval Research
800 North Quincy Street
Arlington, VA 22217

Westinghouse R&D Center
1310 Beulah Road
Pittsburgh, Pennsylvania 15235

TABLE OF CONTENTS

MERCURY BROMIDE LASER RESEARCH

J. L. Pack, C. S. Liu, D. W. Feldman and I. Liberman
Westinghouse R&D Center
Pittsburgh, Pennsylvania 15235

1. INTRODUCTION AND SUMMARY

This report summarizes research work performed at the Westinghouse
R&D Center under ONR/NOSC Contract No. N00014-80-C-0604 "Mercury Bromide
Laser Research", for the period between July 1, 1980 and March 31, 1981.
The major effort was to build a discharge tube and associated apparatus
capable of withstanding temperatures to $300^\circ C$ and pressure to 150 psia,
and to parameterize the HgBr laser fluorescence and laser output with
respect to nitrogen and Ne buffer gas densities. Prior parameterization
has been limited to buffer gas densities of about 1.3 Amagat since the
laser tube was made of Pyrex and therefore could not sustain more than
about 15 psi internal over pressure. By enclosing the Pyrex laser tube
inside a stainless steel pressure vessel, we have overcome this pressure
limitation by maintaining a positive external pressure upon the laser tube.
The steel tank was pressurized with nitrogen to avoid oxidation of the
tube connections. Thus, the discharge tube, by being enclosed in a
nitrogen protective atmosphere, withstands both the high temperature
operation and the high internal operating pressures.

Fluorescence, laser output, voltage and current waveforms were
taken at various nitrogen fill pressures up to 300 Torr with Ne buffer
gas densities up to 5 Amagat. For our experimental tube, the HgBr
laser output and fluorescence efficiency was maximum at a nitrogen fill
pressure of 150 Torr and increased with neon buffer gas density up to the
maximum tested of 5 Amagat at a reservoir temperature of about $150^\circ C$.

2. EXPERIMENT AND RESULTS

A preliminary parameterization of the HgBr laser system limited to buffer gas densities of 1.3 Amagat is described in a Westinghouse internal report entitled "Parameterization Studies of Discharge Excited HgBr System" by J. L. Pack, D. W. Feldman, C. S. Liu and I. Liberman R&D Memo 80-1C2-EXLAS-M1 (see Appendix 1). The work reported here covers only the experiments performed with a pressurized tank at extended buffer gas densities.

A self-sustained glow discharge was obtained in $HgBr_2$ vapor with nitrogen pressures up to 300 Torr and Ne buffer gas densities up to 5 Amagat at a reservoir temperature of about 155°C. These pulsed transverse discharges, preionized by a UV spark source placed behind a screen cathode, were diffuse and had dimensions of 30 cm length x 1 cm gap x 0.3 cm width ($V = 9$ cm^3).

A. Laser Tube

The discharge tube was fabricated from Pyrex including the two windows glass blown to each end at the Brewster angle for optical measurements along the tube length. Electrical feedthroughs consisted of conventional uranium glass transitions and tungsten leads as shown in Fig. 1. The electrodes are molybdenum. Four electrical feedthroughs connected to the anode and the screen cathode (exiting through the bottom of the tube not visible in Fig. 1) provided low circuit inductance. The temperature of the reservoir (coldest spot) located at the bottom of the laser tube determined the vapor density of the $HgBr_2$. Heaters around the windows and along the body of the tube prevented condensation of the $HgBr_2$ elsewhere in the system.
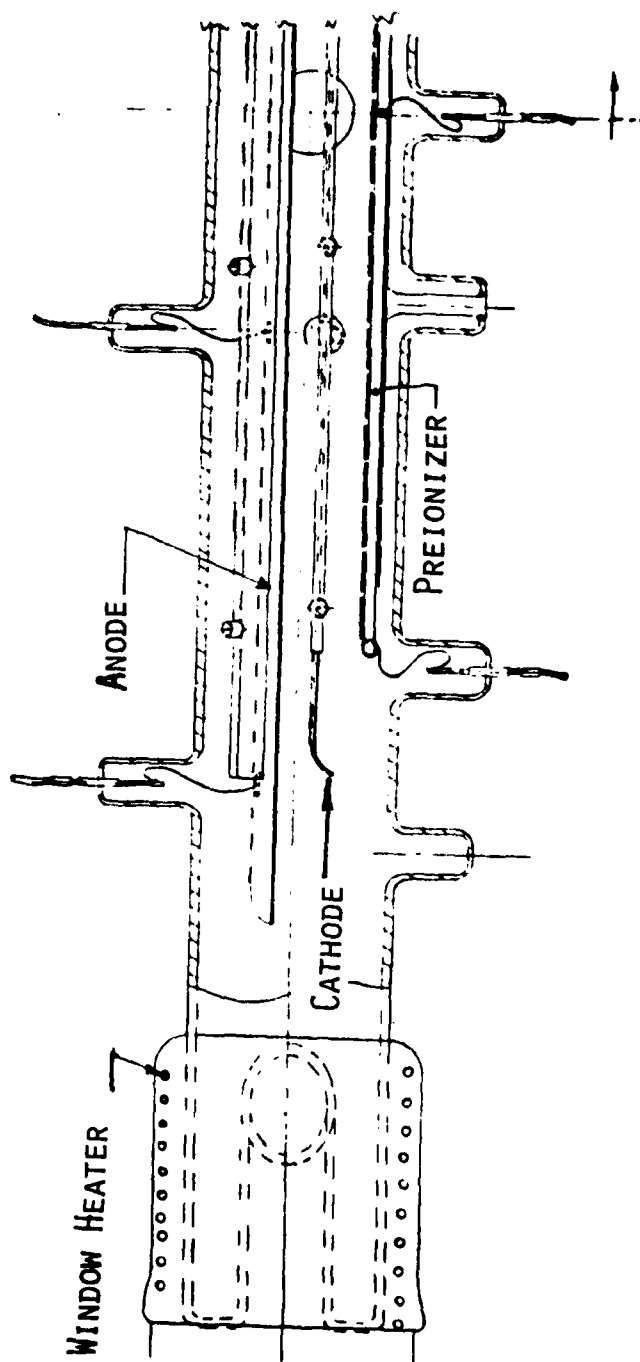
WINDOW HEATER

ANODE

CATHODE

PREIONIZER

Fig. 1. HgBr discharge tube with preionizers behind the screen cathode.

3

B. Pressure Tank

The high pressure tank is made of 1/2-inch thick wall, 14-inch diameter stainless steel pipe with two flanged end plates shown in Fig. 2. This vessel, qualified for operating pressures up to 250 psia, can contain discharge chambers up to 1 m in length operating at temperatures up to 1000°C. The gas species and pressures were controlled through a valve mounted external to the steel tank. We maintained a few psi over-pressure on the Pyrex discharge tube when it was pressurized. All electrical feedthroughs, a pressure inlet for the spark gap and an AR coated window are mounted on one end plate, as shown in Fig. 2. The gas inlet and outlet and a second AR coated window are mounted on the other flange. These second set of gas inlets mentioned above were installed in the flange shown in Fig. 2 after the photograph was taken. The optical cavity extends outside of the pressure tank in order that alignment can be made simplified when the tube is under pressure and at operating temperature. Alignment must be corrected when the tube is pressurized due to refraction by thermal gradients through the hot buffer gas.

C. Circuitry

Since HgBr laser excitation requires very short duration current pulses, the circuitry was made as compact as possible. The capacitors, inside the tank, were mounted just outside the insulating bricks surrounding the heated discharge tube. The final arrangement of components is shown in Figs. 3 and 4. A specially designed spark gap, having identical dimensions to one of the 2.7 nF/40 kV ceramic capcitors, switched the capacitors in the inversion circuit. The capacitors located in the top of Fig. 4 drive the preionizer circuit and were switched by a thyratron external to the high pressure tank. The row of preionization capacitors totaling 30 nF charged to 10 kV produced a 800 A preionization current pulse lasting about 1 μsec. The inversion capacitors (C) consisted of from 3 to 12 2.7 nF/40 dV ceramic capacitors connected in parallel mounted with the spark gap inside the tank as shown in Figs. 3 and 4. The spark gap was triggered just as the preionization current
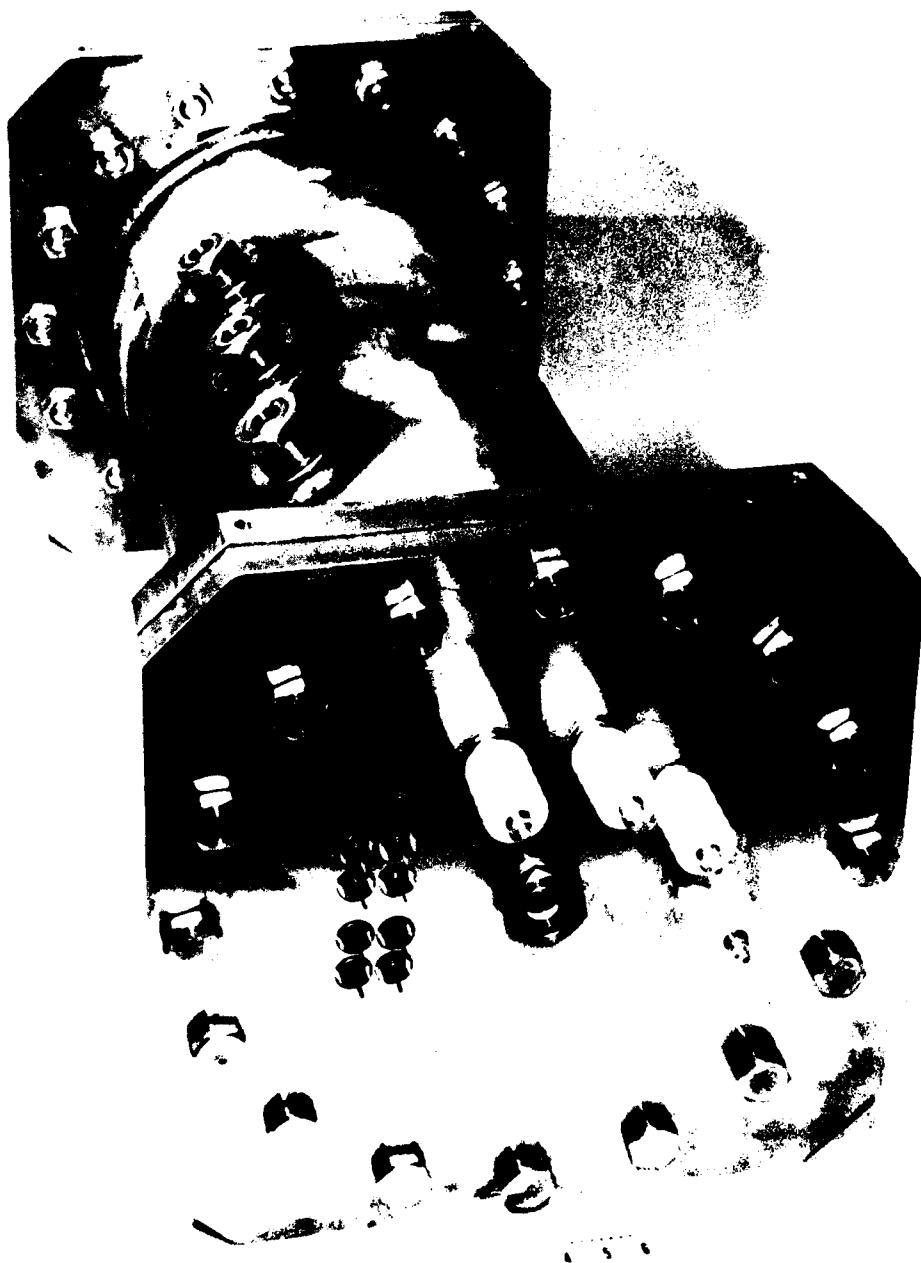
4

Fig. 2. High pressure vessel employed to contain UV-
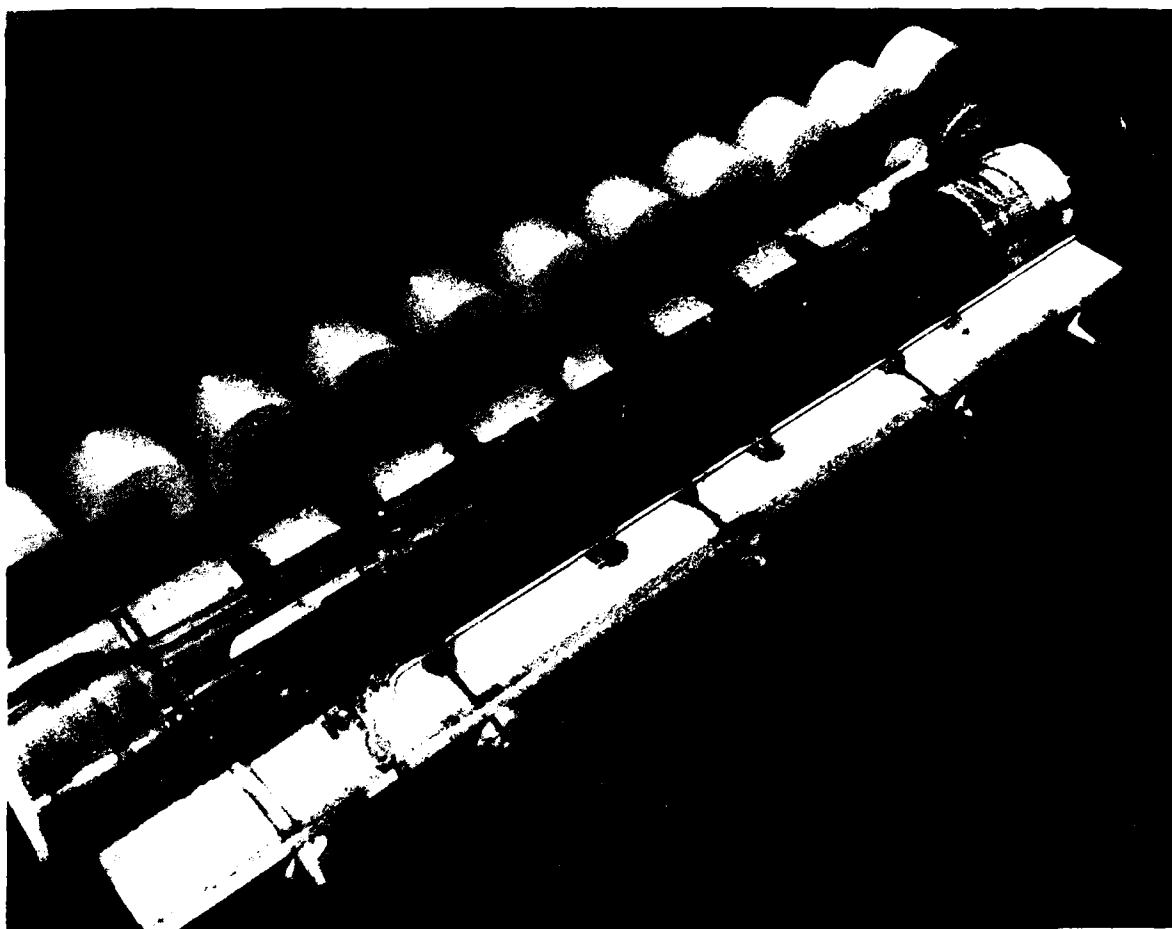preionized, transverse HgBr laser discharges.

5

Fig. 3. Laser tube mounted inside oven with inversion circuit connected prior to installation of preionizer circuit.
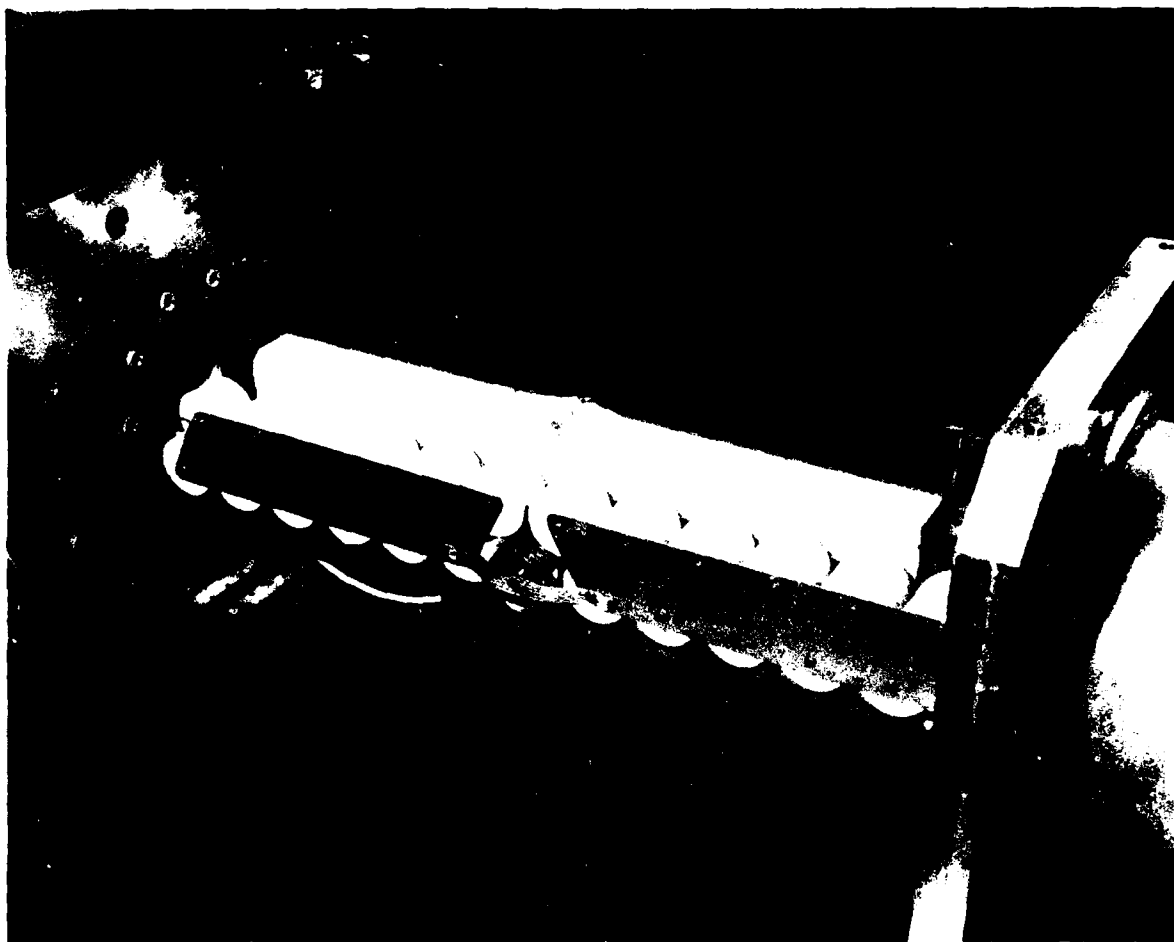
Fig. 4. Oven completed with preionizer circuit mounted ready for installation into high pressure tank.

was decaying to zero. The charging voltage for the main discharge capacitors varied from 15 to 30 kV. The operation of the circuit is conventional.[1] A lead connected to one of the terminals to the anode provided a convenient test point for monitoring the discharge voltage. A Pearson current transformer encircling the lead to the thyratron gave us a measure of the preionization current. The voltage drop across a 0.15 ohm resistance bank in series with the cathode as shown in Fig. 5 monitored the main discharge current. The 0.15 ohm resistance bank consisted of 20-3.0 ohm-1 watt carbon composition resistors arranged in a low inductance configuration. Current and voltage waveforms were displayed on a Tektronix 7834 storage oscilloscope.

D. Electrical Measurements

Due to the inductance of leads, the measured voltage waveform included an inductive component in addition to the discharge voltage and, consequently, tended to reflect the voltage on the capacitors rather than that of the discharge tube. Typical waveforms obtained are shown in Fig. 6. For this example the inversion capacitances (C) were 10 nF, the charging voltage was 25 kV, the cold spot temperature was 150°C (which produced a $HgBr_2$ pressure of about 3 Torr), the nitrogen fill pressure was 100 Torr (at 300°K) and neon was added to give a total gas density of 2 Amagat in the system. Where $di/dt = 0$ we infer that the voltage across the discharge was about 5 kV since reactive voltages are zero at that time. About 10 ns later the measured voltage drops to zero due to the Ldi/dt term in the circuit. Assuming that the voltage across the discharge remains constant during this time, we can calculate the inductance included between the voltage test point and ground to be approximately 200 nh. This was consistent with the physical size of the current loop. Subtracting out the voltage due to this Ldi/dt term from the measured voltage we obtain the calculated discharge voltage waveform shown in Fig. 6. For a more detailed description of voltage and current measurements and an improved current shunt see Appendix 2. The energy into the discharge, computed by integrating the instantaneous voltage current product is about 2.8 Joules. The energy stored on the capacitors
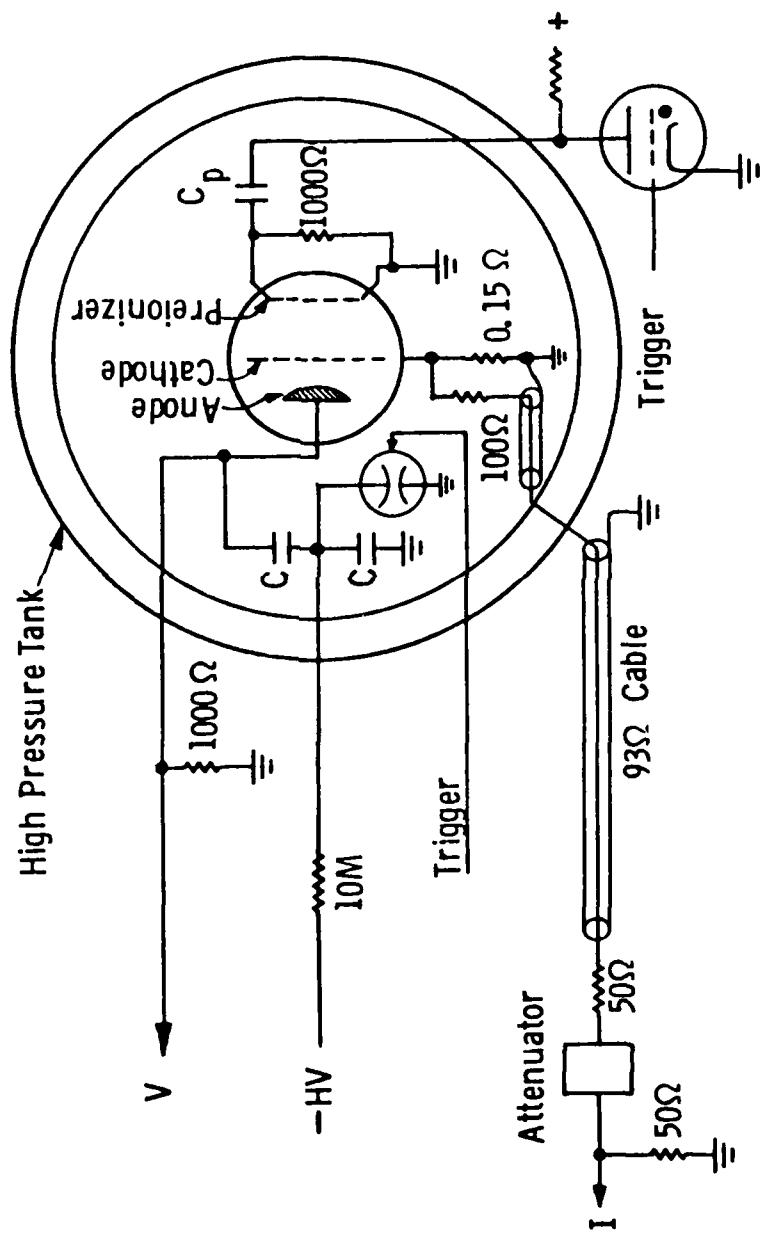
8

Dwg. 7743A96

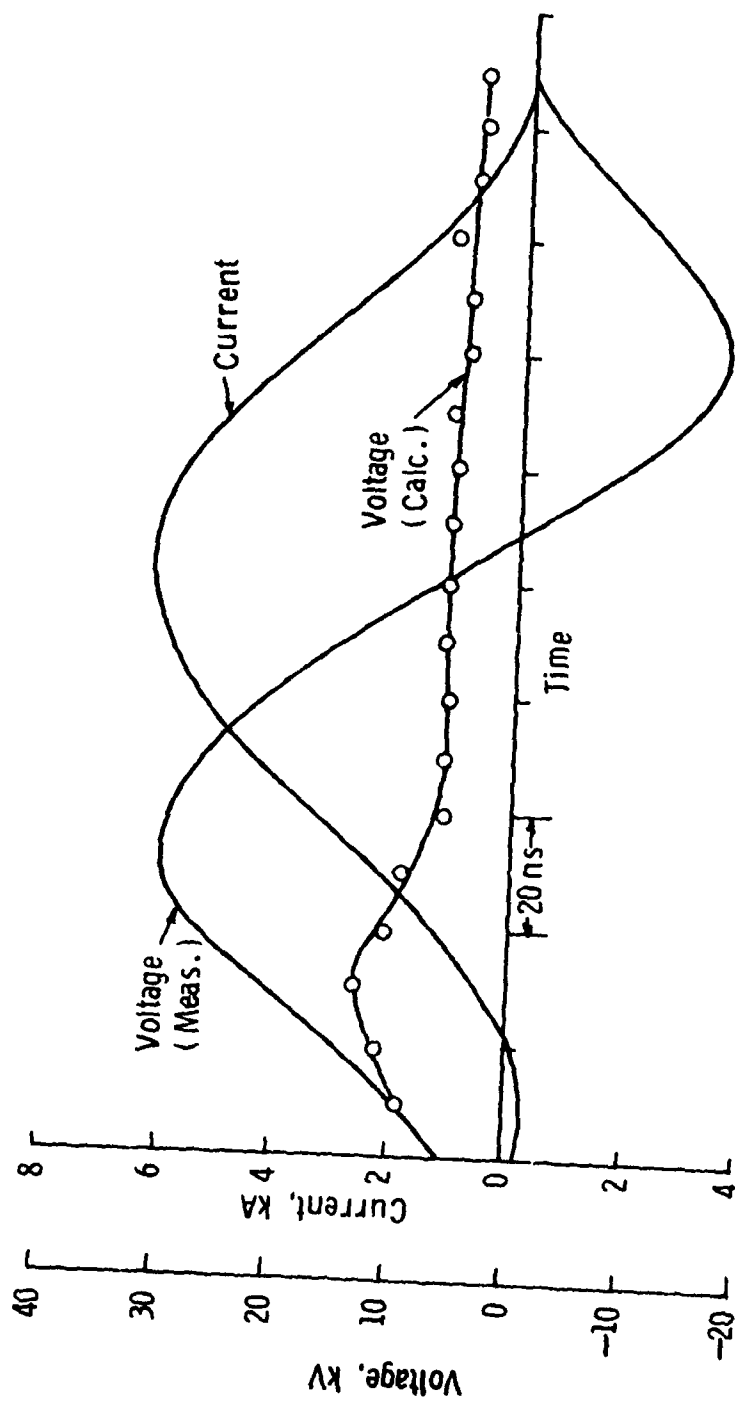Fig. 5. Simplified circuit diagram.

9

Curve 725605-A

Fig. 6. Mercury bromide discharge characteristics.

10

was about 6.25 Joules (10 nF charged to 25 kV). The room temperature value of the inversion capacitors was 17.4 nF for the example shown, but degraded to 10 nf at the operating temperature of 150°C to 160°C. The circuit was very mismatched since over half of the stored energy was dissipated in the spark gap and in subsequent ringing of the discharge circuit. The power supply was designed so that its impedance was greater than that of the discharge impedance. This resulted in a constant current characteristic for a given power supply voltage and capacitance regardless of changes in the discharge parameters such as mixture and pressure. The current delivered to the discharge could be varied by changing the charging voltage and/or the capacitances.

Increasing the discharge voltage by increasing the nitrogen or neon buffer gas density tends to improve the matching of the circuit. These effects are shown in Fig. 7 where the discharge voltage is shown as a function of total gas density in Amagat for various nitrogen pressures at room temperature and at 435°K. As shown, the effect of heating the gas up to 435°K was negligible as far as the discharge voltage was concerned since the total gas density changed only slightly due to $HgBr_2$. Increasing the neon density from about 1 Amagat to about 7 Amagat caused the discharge voltage to increase by about 80% for a nitrogen fill pressure of 100 Torr.

E. Optical Measurements

Fluorescence and laser output were measured at various charging voltages, size of capacitances and nitrogen pressures and neon buffer gas density. The fluorescence and laser output waveforms are shown in Fig. 8 for the conditions previously shown in Fig. 6. The laser output typically peaks at the peak of the current waveform; however, the fluorescence always peaked 20 to 60 ns earlier. At lower discharge currents and charging voltages, the fluorescence occurred closer to the peak of the discharge current. We tentatively explain the early peak of fluorescence relative to the current peak as due to quenching of the upper laser level at the high current density necessary for lasing to occur in our experimental tube. The delay in lasing relative to the

11

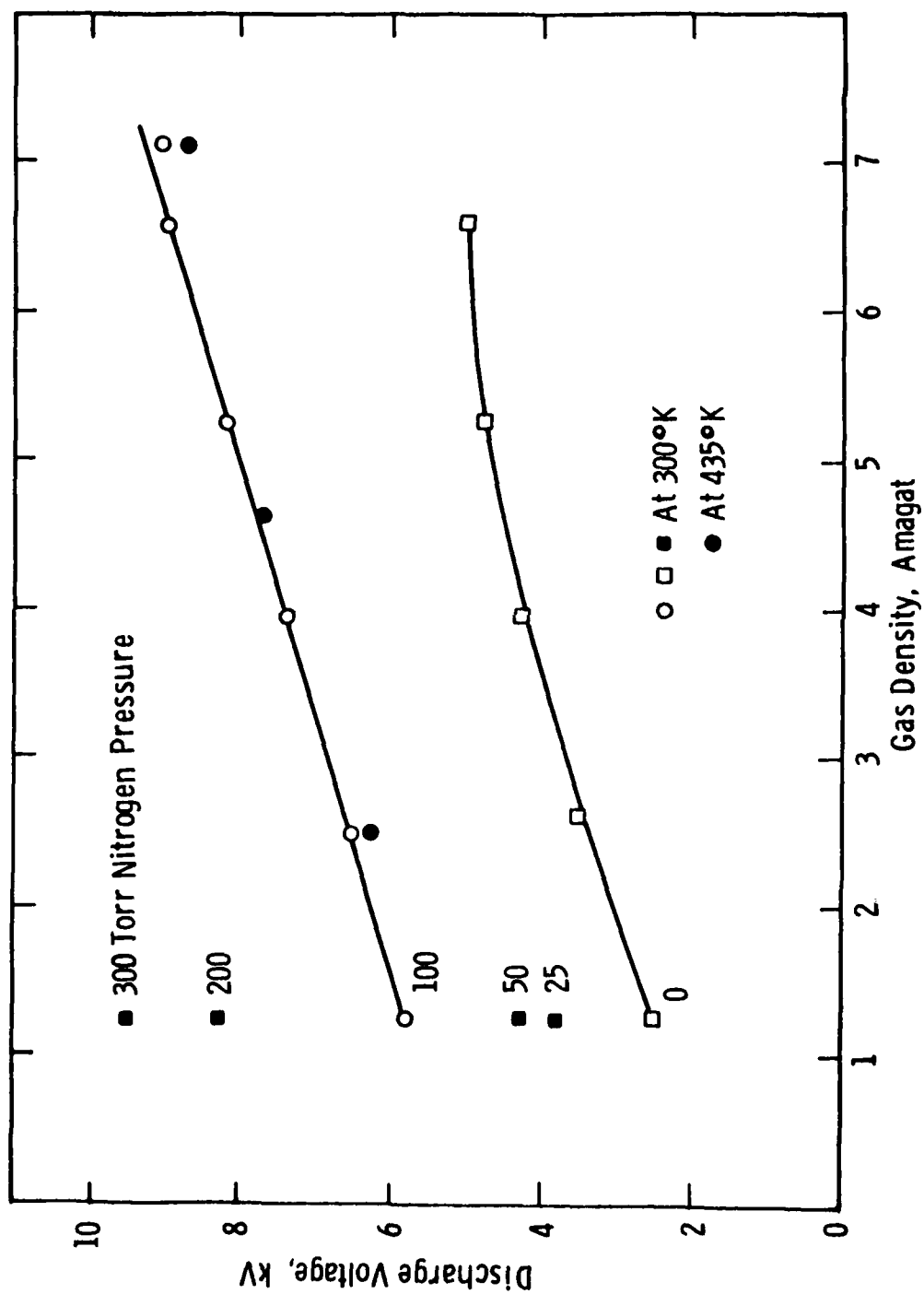Fig. 7. N_2:Ne mixture discharge voltage variation.
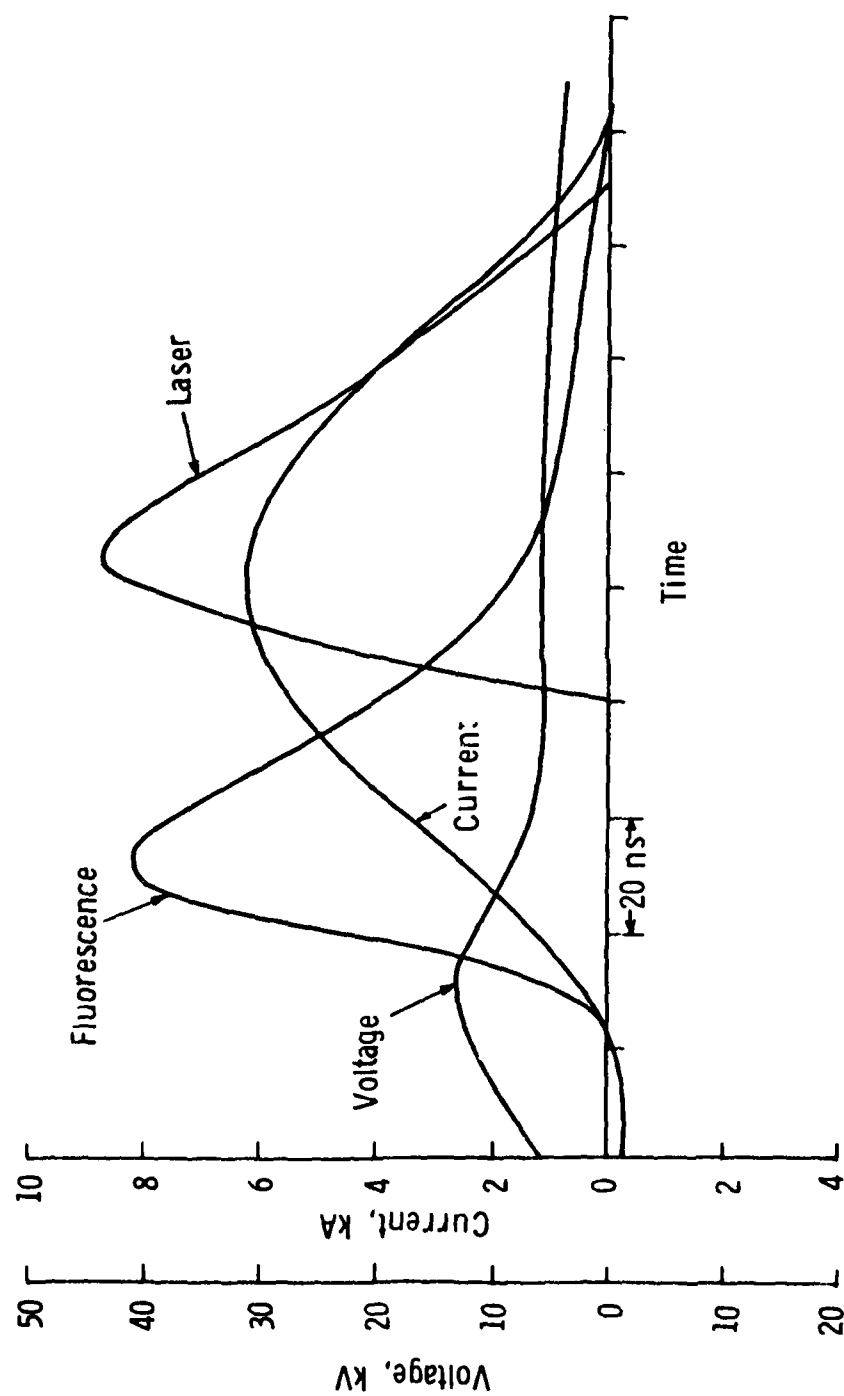
Curve 725604-A

12

Curve 725606-A

Fig. 8. Mercury bromide radiation sequence.

13

fluorescence is difficult to understand but may be a result of high
laser cavity losses (see Section F). The same fast vacuum photodiode
monitored the laser and fluorescence signals. Neutral density filters
served to prevent saturation of the detector during the laser measurements.

F. Laser Output as a Function of Pressure

Using a calibrated fast photodiode and filters mentioned above,
we obtained laser output as a function of total gas density for several
nitrogen pressures using storage capacitances of 10 nF charged to 30 kV.
These results are shown in Fig. 9. The gas temperature was 435°K and
the cold spot temperature was about 10 degrees lower yielding a $HgBr_2$
density of about 10^{17} molecules per cc. Peak laser output occurred for
a nitrogen pressure of 150 Torr and at the highest neon buffer gas density
used (5 Amagat). At this neon density, the output was still increasing
but appeared to be saturating. It was discovered that the Brewster angle
windows gave a large scattering loss due to "bloom" on their surfaces.
This loss of about 25% per pass accounted for the large threshold observed
and resulted in a low overall efficiency. However, the main result is
that the output increased with buffer gas density and optimized at a
nitrogen pressure of 150 Torr.

G. Fluorescence as a Function of Pressure

The fluorescence is a better measure of efficiency of the pumping
of the upper laser level in the pressure of large cavity losses mentioned
above and is shown in Fig. 10 as a function of total gas density for the
same conditions as Fig. 9. Here the current pulses were almost identical
for the different densities so that whatever quenching that occurred is
the same at the various total densities. However, since the glow voltage
does increase with gas density, the fluorescence was normalized to the
energy dissipated in the discharge. Therefore, the increase in fluorescence
with gas density is due to an increase in the efficiency of producing
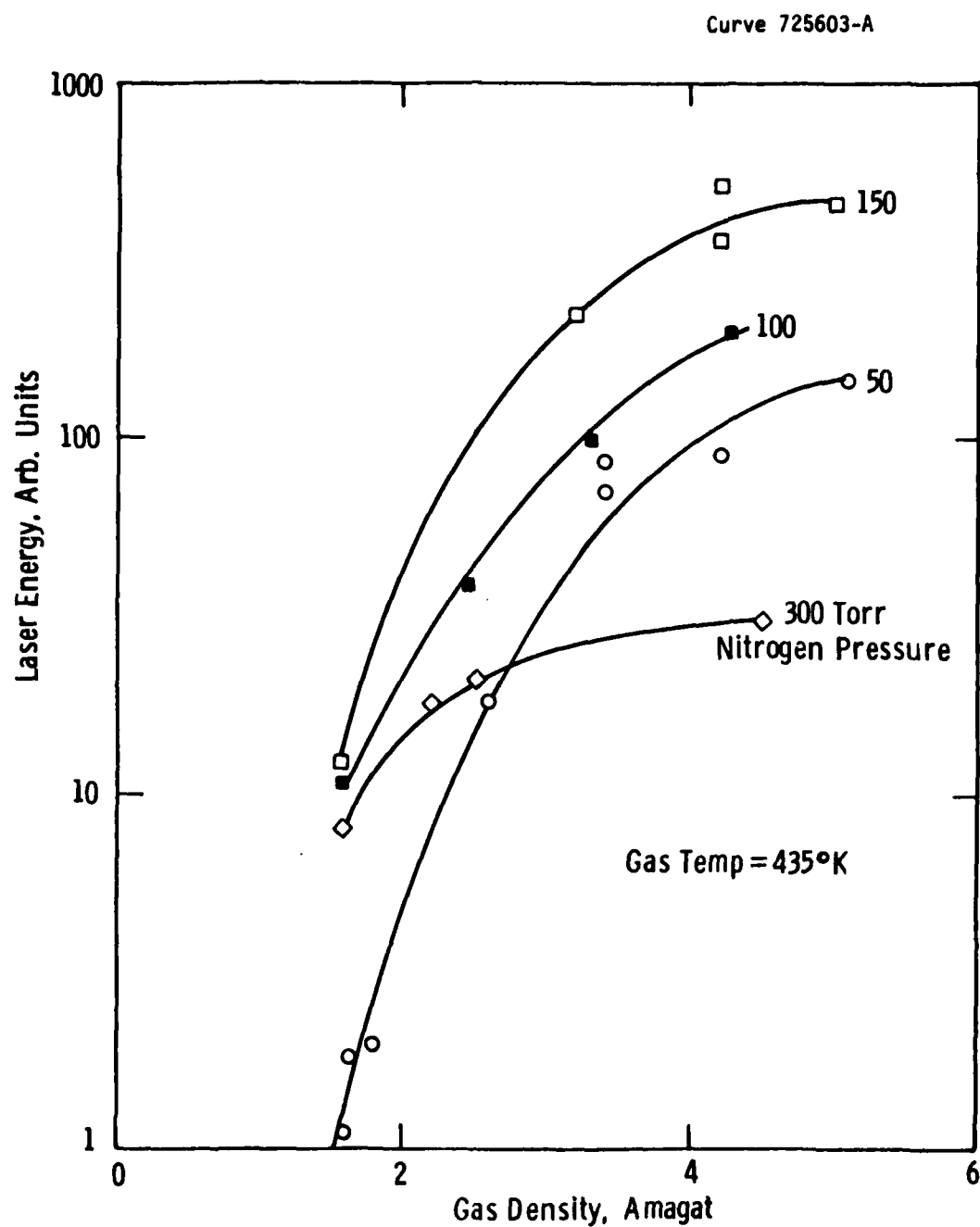upper laser level population.

14

Fig. 9. Laser output versus neon buffer gas density at several nitrogen fill pressures.
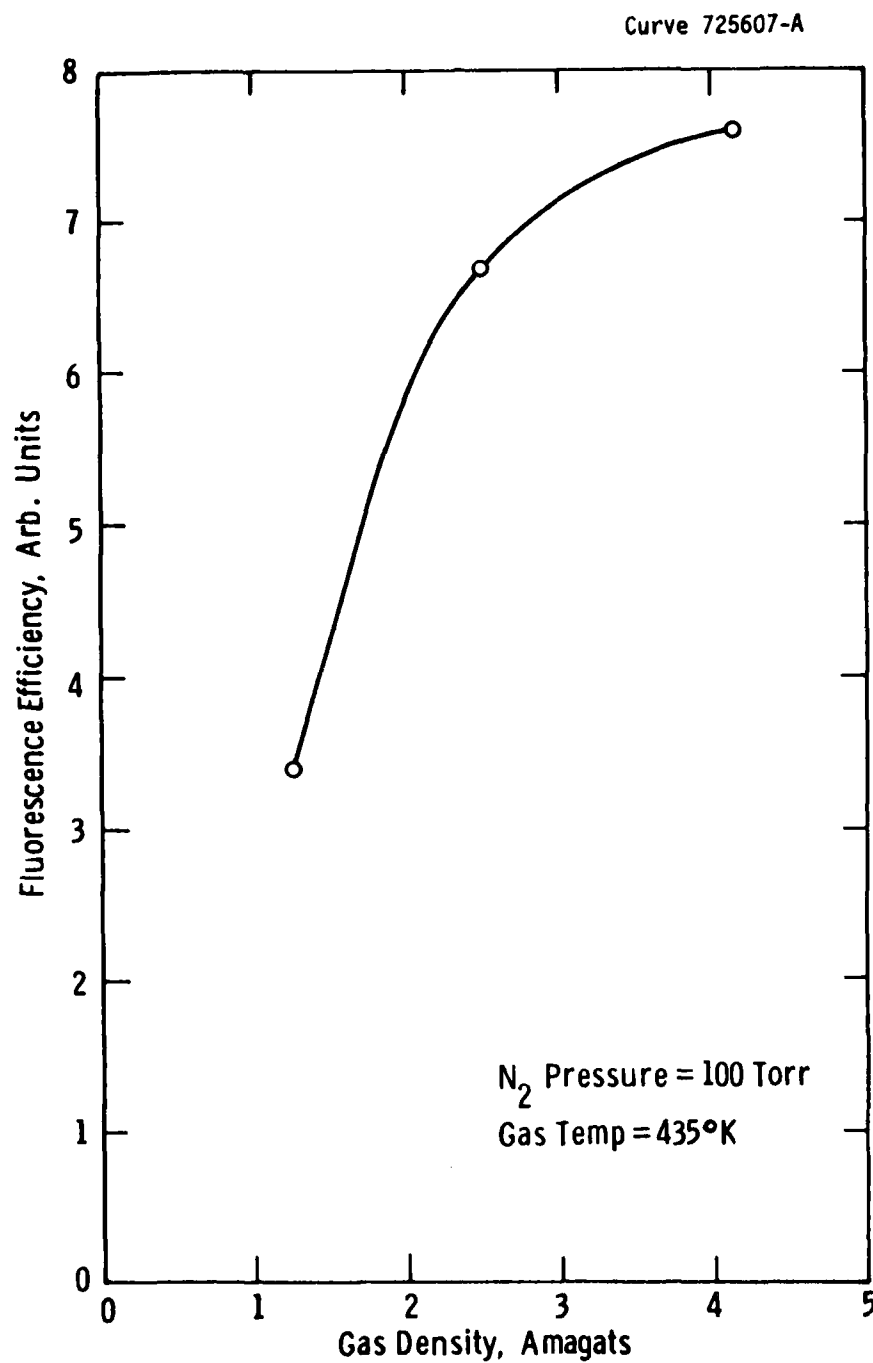
Fig. 10.   Fluorescence efficiency versus total gas density.

16

H. Laser and Fluorescence Output as a Function of Storage Capacitance and Charging Voltage

The laser output increased linearly with charging voltage rather than quadradically for charging voltages from 20 to 30 kV. The reason for this is due to the constant discharge voltage characteristics. Due to the constant current characteristics of the power supply, raising the charging voltage increased the discharge current proportionally giving only a linear increase of energy into the discharge with charging voltage. Some data was taken with discharge capacitances equal to 5, 10, and 20 nF. The laser output was roughly proportional to the value of storage capacitance at the higher gas densities for charging voltages well above threshold.

3. CONCLUSIONS AND SUGGESTIONS FOR FURTHER RESEARCH

For our experimental tube, the HgBr laser output and fluorescence efficiency was maximum at a nitrogen pressure of 150 Torr and increased with neon buffer gas density up to the maximum tested of 5 Amagat at a reservoir temperature of 150°C. Due to the large scattering losses at our Brewster angle windows, the output of our laser was much less than expected and does not represent the capabilities of the HgBr system. Increasing the neon density from 1.3 Amagat (where others have obtained a 0.9% laser efficiency) to 4 Amagat increased the fluorescence efficiency in our tube by a factor of 2.4. This improvement will have to be verified with larger tubes.

Recently we have obtained bloom free windows using a frit sealing technique. We propose that a new tube be constructed of quartz having Brewster angle bloom free windows and further parameterization be done with a discharge of greater cross section and length. Higher energies produce a closer approximation to a practical laser. Due to time limitations we did not conduct the study of temperature effects upon laser performance or effects of using other buffer gas species. Further study of these two parameters should undoubtedly lead to a more optimized $HgBr_2$ laser system. The reason for the recommendation that quartz be used is based upon our experience with the superior reliability of quartz feedthroughs over the Pyrex uranium feedthrough used in the discharge tube of this study. Based on this present study we believe that implementating the above suggestions would result in a demonstration of laser efficiency in excess of 2%.

4. REFERENCES

1. E. J. Schimitschek and J. E. Celto, "Mercuric Bromide Dissociation Laser in an Electric Discharge," Optics Lett. 2(3), March 1978.

This report was typed by Sandra V. Brown.

5. ACKNOWLEDGMENT

The authors gratefully acknowledge the expert technical assistance of R. K. Williams and L. Jasper and helpful discussions with S. G. Leslie

APPENDIX 1

PARAMETERIZATION STUDIES OF DISCHARGE EXCITED HgBr LASER

J. L. Pack, D. W. Feldman, C. S. Liu and I. Liberman
Westinghouse R&D Center
Pittsburgh, PA. 15235

1. INTRODUCTION

Westinghouse has obtained an 8-month program to study the HgBr laser system. The effort concentrates on parameterizing discharge excited HgBr lasers, using existing TlHg high pressure experimental apparatus. Prior to using the high pressure system preliminary parameterization studies have been made up to 1000 Torr which is the subject of this memo.

During the past several years, mercury bromide has shown great promise as a high efficiency, high energy tunable laser in the blue-green region of the spectrum. Lasing in this medium has been demonstrated using a number of excitation techniques: optical pumping,[1] E-beam,[2,3] E-beam sustained discharge,[4,5] and self-sustained discharge.[6,7] The most promising technique thus far seems to be a UV-preionized self-sustained discharge, which has demonstrated energies of 400 mJ,[8,9] and efficiencies of ~1 percent.

Although there has been some speculation about the details of the excitation and lasing kinetics, optimization of this laser system still depends on empirical parameterizations. Optimization studies made to date were limited by the apparatus available. A number of important questions remain: for example, the independent effect of temperature and of $HgBr_2$ density, and the effect of buffer gas density on laser kinetics and discharge characteristics.

1

Attempts to establish parameters for a number of variables in
the mercury bromide system have been severely limited in range. Buffer
gas pressures have extended up to ~1 amagat, with temperatures up to
~200°C and $HgBr_2$ densities to $5 \times 10^{16}/cm^3$. This range of parameters
has been determined basically by the type of apparatus used: that is,
O-ring seals, simply Pyrex structures, and stainless steel electrode
materials. The density of $HgBr_2$ has been adjusted by varying the tem-
perature of the laser tube; thus the gas temperature and the $HgBr_2$
density were not independent variables. Both the temperature and
pressure affect the laser kinetics, through the collision rates, for
instance. In addition, the buffer gas density affects the discharge
characteristics by changing both the E/N and the glow voltage. As the
length of the discharge region is increased to produce larger volumes,
the discharge impedance decreases; it would be advantageous to increase
the impedance by increasing the buffer gas density.

In this program the buffer gas density, temperature, and energy
loading will be varied independently, so as to optimize the performance
of the HgBr laser. This memo covers a preliminary parameterization
procedure whereby the buffer gas pressure was limited to approximately
2.2 atmospheres absolute. The next phase in which use is made of the
TlHg experimental apparatus is scheduled to begin during August, 1980.

2. TECHNICAL DISCUSSION

Laser action on the $B^2\Sigma^+ \rightarrow X^2\Sigma^+$ band of HgBr at 502 nm has been observed independently by several investigators.[1,2,6] This bound-bound laser transition originates on the first electronic state, $B^2\Sigma^+_{1/2}$, of the HgBr molecule at v' = 0 and terminates on the $X^2\Sigma^+_{1/2}$ state at v" = 22. The large Franck-Condon shift of the B → X states suggests that, for pulsed excitation, bottlenecking of the lower laser level is minimal, given rapid deactivation of the X-state v" = 22 level through collisional quenching at high buffer gas pressures. In high pressure operation, collisional relaxation rates are sufficiently rapid that the vibrational states in the upper and lower levels are in thermal equilibrium at the gas kinetic temperature. Thus the quasi-static theory of line broadening can be used to predict stimulated emission and absorption coefficients as a function of wavelength for a given temperature. Equilibrium calculations (Table 1) of chemical species in $HgBr_2$ vapor in the absence of excitation indicate that at temperatures below 700°K, the concentration of HgBr ground state molecules dissociated thermally is less than 10^{-10} of the $HgBr_2$. Since HgBr laser transitions occur from the potential minima of the excited molecular states, the corresponding ground vibrational states are not excessively populated at these gas kinetic temperatures. Thus thermal population of the terminal laser levels is not expected to be a problem in thermally equilibrated $HgBr_2$/HgBr mixtures.

A significant advance in HgBr laser technology was recently achieved by Schimitschek[8] of NOSC, whose UV-preionized discharge excitation demonstrated energies of ∿100 mJ and efficiencies of ∿1 percent. However, it is by no means clear that the performance of the HgBr laser system has been optimized. The actual excitation and deactivation mechanisms of the HgBr upper and lower laser levels remain uncertain.

Table 1 — Vapor Densities of $HgBr_2$, $HgBr$, Hg, Hg_2, and Br
As Calculated from Thermodynamic Equilibrium Conditions

Temperature (°K)	Particles/cm³					
	$HgBr_2$	$HgBr$	Hg	Hg_2	Br_2	Br
450	1.67×10^{17}	4.10×10^1	3.26×10^{10}		3.29×10^{10}	2.58×10^6
500	1.30×10^{18}	1.34×10^4	9.23×10^{11}		9.23×10^{11}	1.73×10^8
700	6.02×10^{20}	7.10×10^{10}	7.29×10^{15}		7.29×10^{15}	1.02×10^{13}
800	6.02×10^{20}	2.02×10^{12}	4.52×10^{16}	9.4×10^{11}	4.51×10^{16}	1.92×10^{14}
900	6.02×10^{20}	2.85×10^{13}	1.85×10^{17}	1.36×10^{13}	1.84×10^{17}	1.87×10^{15}
1000	6.02×10^{20}	2.29×10^{14}	5.68×10^{17}	1.15×10^{14}	5.63×10^{17}	1.15×10^{16}

There has been some speculation about the details of the excitation and lasing kinetics, but optimization of this laser system to date has been empirical and limited by the apparatus available. A number of important questions remain: for example, the effect of buffer gas species and pressure, and the effect of $HgBr_2$ density on laser kinetics and discharge characteristics.

The ultimate goal of this study is to optimize the performance of HgBr lasers with respect to internal gas conditions.

2.1 HgBr Laser System Design

The HgBr laser discharge tube design was guided by two fundamental considerations: the rapid deactivation of the lower laser level through collisional quenching at high buffer gas pressures, and the fairly high temperature operation (150 to 300°C) required by possible high $HgBr_2$ vapor density. The optimization of the HgBr laser may require operation of the discharge cell at high $HgBr_2$ density and high buffer gas pressures. Therefore, a discharge tube which will withstand both high temperatures (~300°C) and high pressures (150 psi) was built.

4

As is well known from previous experience, the chemical compatibility of $HgBr_2$ is a most important factor in material selection. Both glass and tungsten or molybdenum are known to be inert to $HgBr_2$, Hg, and Br_2, even at elevated temperatures. In previous laser development efforts, we developed reliable glass-tungsten and quartz-molybdenum high-temperature seals which were used in fabricating the all-hot clean laser cell.

The electrodes are molybdenum. Preionization sparks are placed behind a screen anode, as shown in Figure 1. The active volume is about 0.3 cm wide by 1 cm gap by 50 cm long. Four electrical feedthroughs connected to the screen are employed to minimize the circuit inductance. The vapor density of the $HgBr_2$ is temperature controlled by a reservoir located at the bottom of the laser tube. The buffer gas species and pressures is externally adjusted through a bakeable valve. The whole laser tube is designed to be self-contained; its optical cavity can be mounted directly onto the laser tube as shown in Figure 1.

Since HgBr laser excitation requires an electrical current pulse with ultra-fast risetime ($\sim$30 ns), very short duration ($\sim$100 ns), and high peak amplitudes (> 100 A cm^{-2}), the laser tube and circuitry must be designed with minimum inductance. To accomplish this a Blumlein type pulser is placed close to the laser tube. This circuit, shown in Figure 2, minimizes the inductance and eliminates the switch from the discharge circuit. Two spark gaps are used in this circuit, one to operate the preioinizer and the other to invert half the capacitors in the main discharge storage bank C_1-C_{24}. The preionizer is driven by 2 capacitors C_{25} and C_{26}. By adding inductance in series with C_{25} and C_{26} the preionization current pulse length can be adjusted to provide satisfactory performance. Increasing the preionization capacitors to 21.6 nF gave more uniform discharges, however, the pulse width had to be increased to about 2 µsec to avoid arcing to the screen. This required a longer delay, therefore, an adjustable delay generator was used instead of the original 100 ft RG8/U cable to delay the dischrage pulse with respect to the preionization pulse. Four 1-ft long 3.6 ohm strip lines
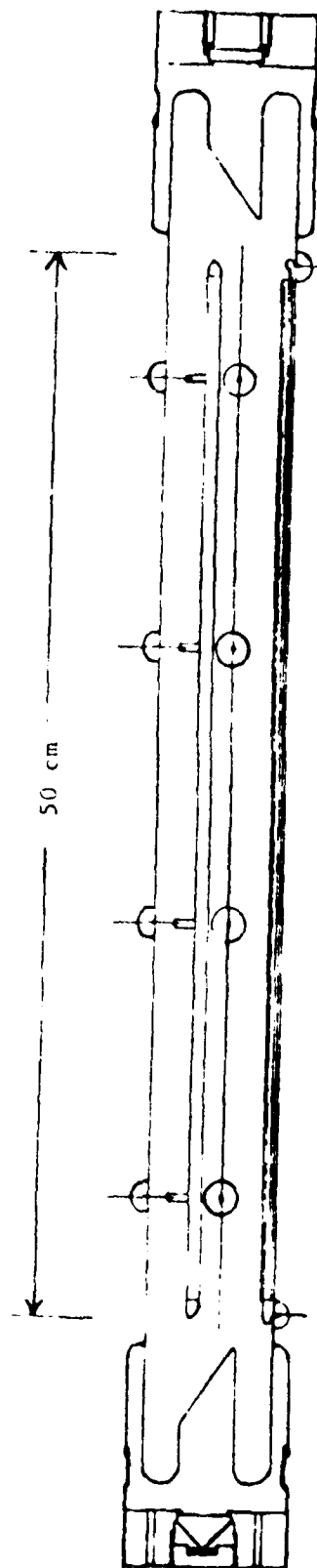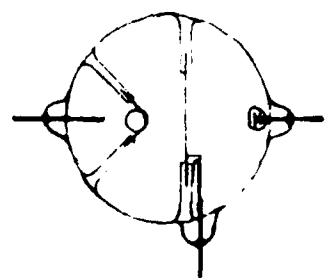
Fig. 1 — HgBr discharge tube with preionizers behind the screen anode

Fig. 2 — Blumlein type pulser and preionizer circuitry

7

provide low impedance connections from the main capacitor bank through the wall of the oven to the 4 feedthroughs that are connected to the screen electrode. A high voltage probe connected to the end of one of the strip lines is connected to the discharge tube provides voltage monitoring of the dischrage. The stainless steel ground return for 2 of the strip lines has a resistance of about .03 ohms which provided a convenient test point for monitoring the current.

The preionizer power supply was adjusted to about 10 kV. Main discharge power supply voltages from 8 to 20 kV gave good glow discharges. Voltage and current waveforms obtained with a 16 kV main discharge supply voltage are shown in Figures 3a and 3b. In Figure 3a the discharge voltage, current are shown just following the preionization current pulse of 400 A lasting 2 μsec. The adjustable delay generator allowed us to optimize the timing of the discharge pulse with respect to the preionization pulse. The main voltage and current waveforms are shown on an expanded time scale in Figure 3b. The discharge voltage rises to about 17 kV before breaking down then falls to about 6 kV at the peak of the discharge current. The discharge current peaked at over 6000 A which represents a current density of about 300 A/cm^2 since the discharge appeared to be only about 3 mm wide.

The discharge current pulse width of 150 ns is consistent with a circuit inductance of 0.14 μH which is about as low as the present tube design can achieve.

2.2 Optimization of HgBr Lasers

The behavior of $HgBr_2$ discharges has not, to date, been studied sufficiently to allow for predictions of what $HgBr_2$ density, buffer gas pressure, and temperature will be required for optimal laser conditions. Past experience with excimer lasers, however, indicates that a high buffer gas pressure will be beneficial to the HgBr laser operation, for three reasons: (1) rapid deactivation of the lower laser level, (2) capability for higher energy loading, and (3) better impedance matching
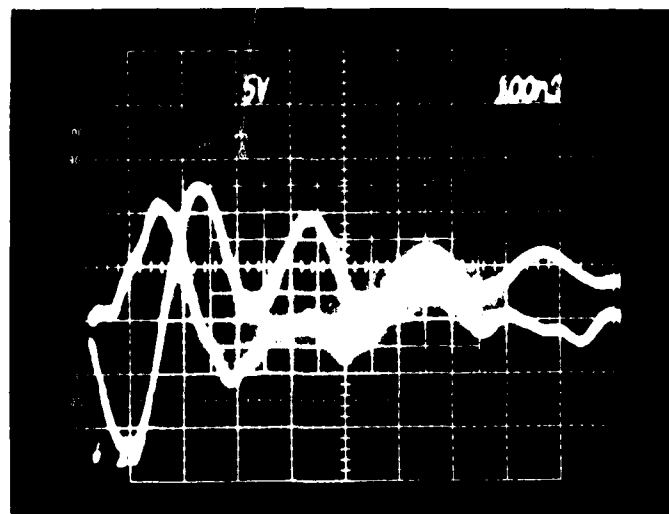
8
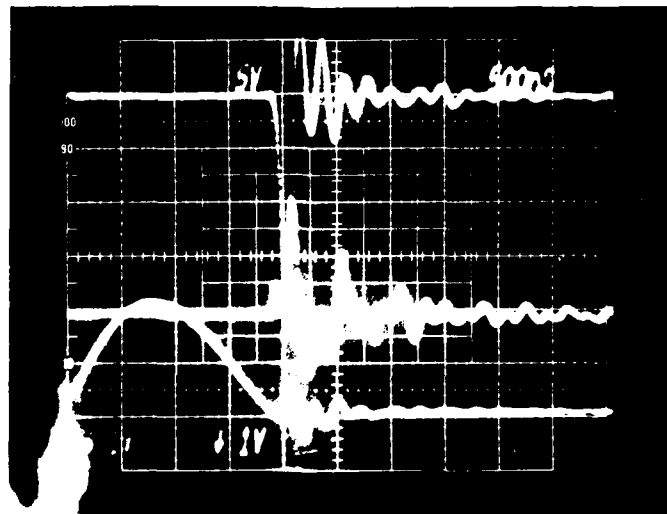
↓V, 5 kV/div

↑I, ∿2900 A/div

I_p, 200 A/div

Fig. 3a – Discharge voltage, current and preionizer current waveforms for 14 kV charging voltage.

— ↓V, 5 kV/div

I, 2900 A/div

Fig. 3b – Discharge voltage and current waveforms at 100 nsec per division

9

to pulser circuits. Higher $HgBr_2$ vapor density should always be helpful to the HgBr laser, provided that it will not affect the discharge and that the $HgBr_2$ molecules will not de-excite the upper laser level significantly. The temperature effect on the HgBr laser kinetics is totally unknown. Thermal dissociation of $HgBr_2$ and/or temperature dependence of reaction rates can be either beneficial or detrimental. The optimization must, therefore, be empirical.

Figure 4 shows a simplified overall layout of the apparatus used to perform the preliminary optimization of the HgBr system. The oven is multiply temperature controlled so that the ends are kept hotter than the central region. Since the pressurized oven was not used for these experiments the temperature sensor-pressure regulator-N_2 tanks were not employed.

Both axial and transverser fluorescence was monitored using a light pipe to input to the monochromator which coupled to an optical Multichannel Analyzer (OMA). The OMA provided a complete spectrum each time the discharge tube was fired. A calibrated fast photo diode monitored the energy and duration of the fluorescence and lasing when it occurred.

The spectrum was plotted out on an XY chart recorder and the time dependence of the fluorescence or the laser pulse was displayed on a fast oscilloscope (Tektronix 7834).

Since optimization of the parameters mentioned above depend upon proper initiation of the glow discharge, the first operating parameter optimized was the preionization pulse. As a first choice of buffer gas we chose a known suitable mixture of 900 Torr Ne + 100 Torr N_2.[9] As mentioned above, a preionization energy of about 2 Joules was found to yield uniform discharges. We did not investigate the range between 0.25 Joules and 2 Joules but found 0.25 Joules inadequate to give the uniformity desired. A more detailed search for the optimum preionization energy will be made when using the pressurized tank.
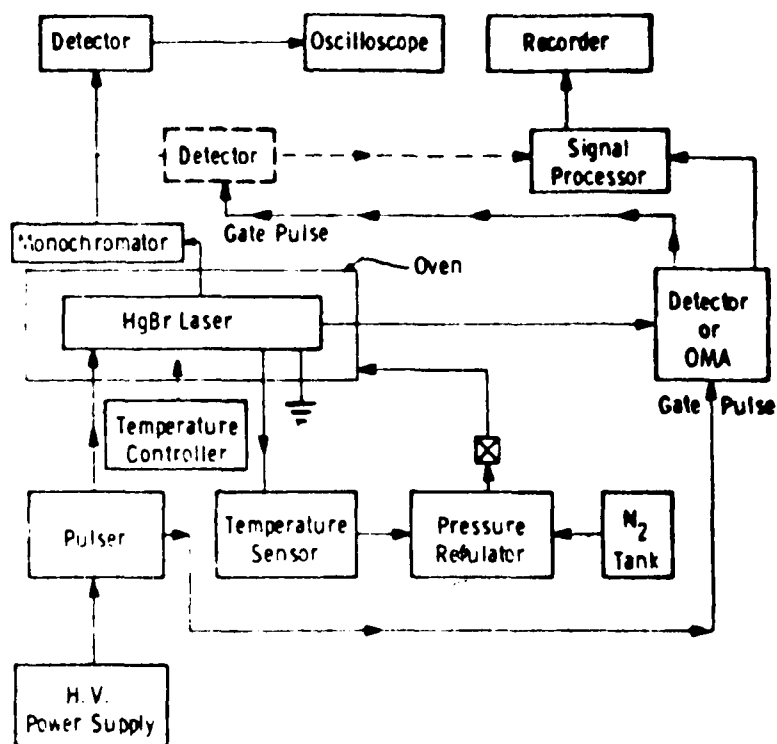
Fig. 4 – Spectroscopic apparatus used to measure the fluorescence of pulsed HgBr discharges

To optimize the delay, the operating temperature was fixed at about 150°C and the delay was varied between the preionization pulse and the discharge pulse. The variation of fluorescence as a function of this time delay for a discharge charging voltage of 16 kV is shown in Figure 5. Here we have the peak time integrated fluorescence signal in arbitrary units from the OMA at about 501.8 nm for one discharge pulse as a function of time delay after the preionization pulse. Zero time delay corresponds to the waveforms shown in Figure 3. Thus, for this choice of preionization the fluorescence exhibits a broad peak lasting about 2 μsec after the preionization pulse. For less preionization energy we would expect less of a "window" as observed by Sze with Rare-Gas halide lasers.[10]

The variation of fluorescence at 501.8 nm as a function of temperature and charging voltage is shown in Figure 6. The flattening of all curves at charging voltages above 14 kV is believed to be due to increasing mismatch of the network at the higher voltages. Since the glow voltage does not change as the charging voltage is increased the network progressively fails to discharge all of its energy during the first current pulse in the discharge.

The spectrum of the fluorescence is shown in Figure 7. The spectrum was qualitatively the same for all temperatures and charging voltages shown in Figure 6. In Figure 7 is shown only the central 500 Å region of the 1500 Å span of the spectrometer used to observe the spectrum of the HgBr discharge. There was no other spectra between 4200 and 5700 Å from the discharge using 900 Torr Ne + 100 Torr N_2 buffer gas. The spectra exhibits many peaks representing different vibrational transitions which were tentatively identified using the extensive tables of Cheung and Cool.[11] The separation of the peaks is 3 to 3.5 nm. The ratio of the intensity at 498.5 nm to that at 501.9 nm ∿ 0.6. Several transitions combine to produce the peaks from higher upper state vibrational levels accounting for the larger ratio of intensities of the neighboring peaks at 488.8, 485.6, 482.5 nm and shorter wavelengths.
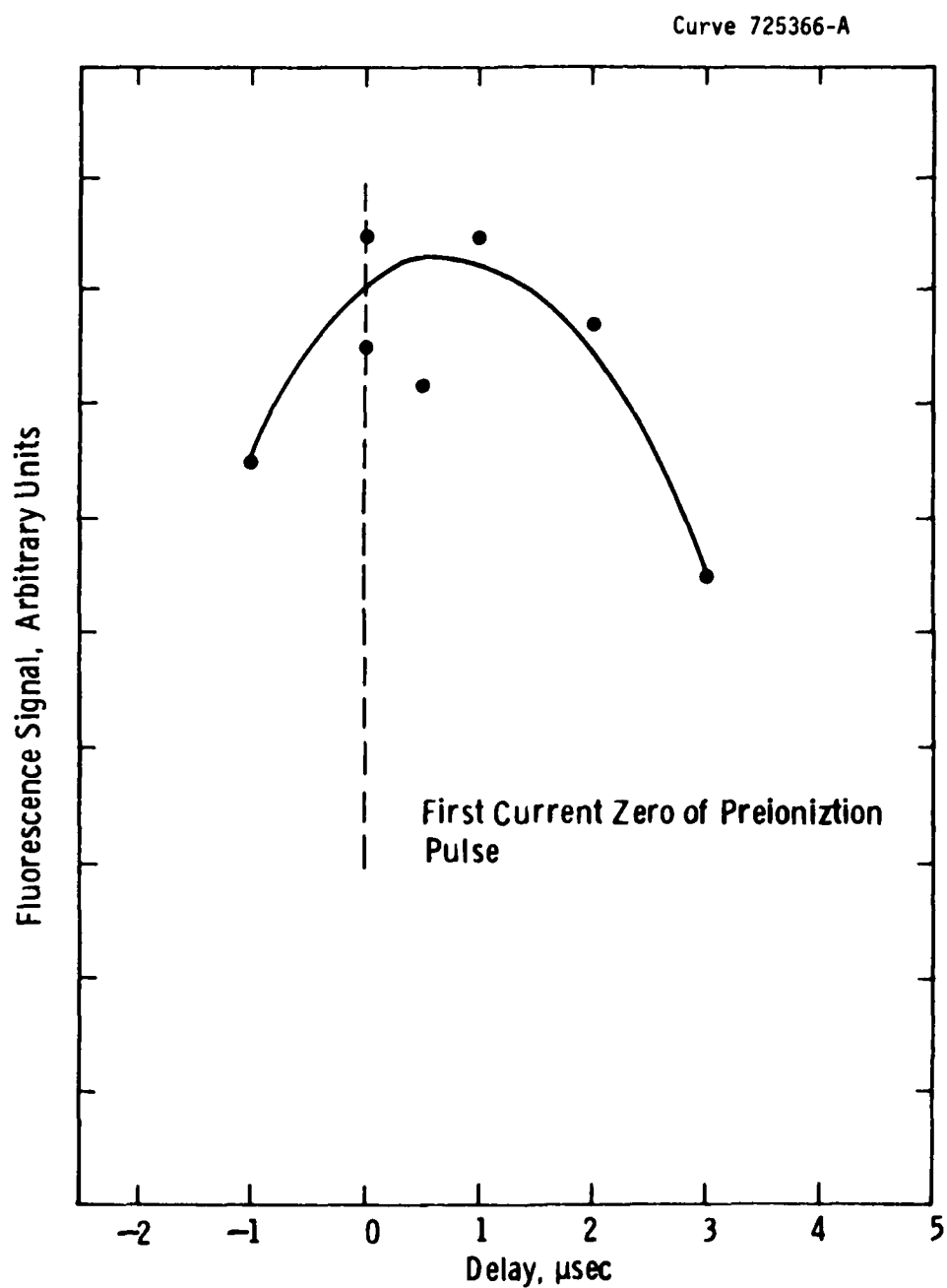
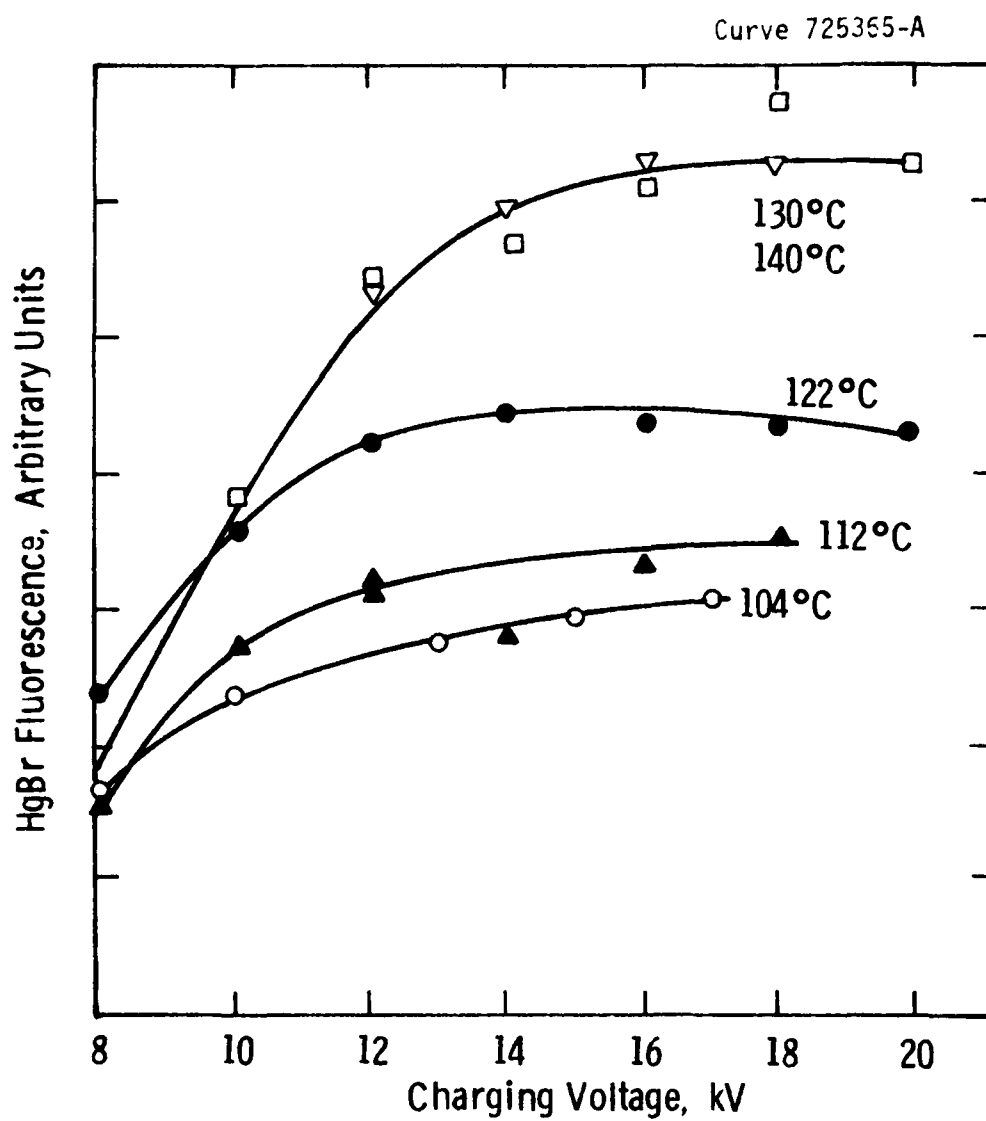Fig.5 — HgBr fluorescence as a function of delay between discharge
current and preionization

Fig. 6 — HgBr fluorescence as a function of capacitor changing voltage at various temperatures
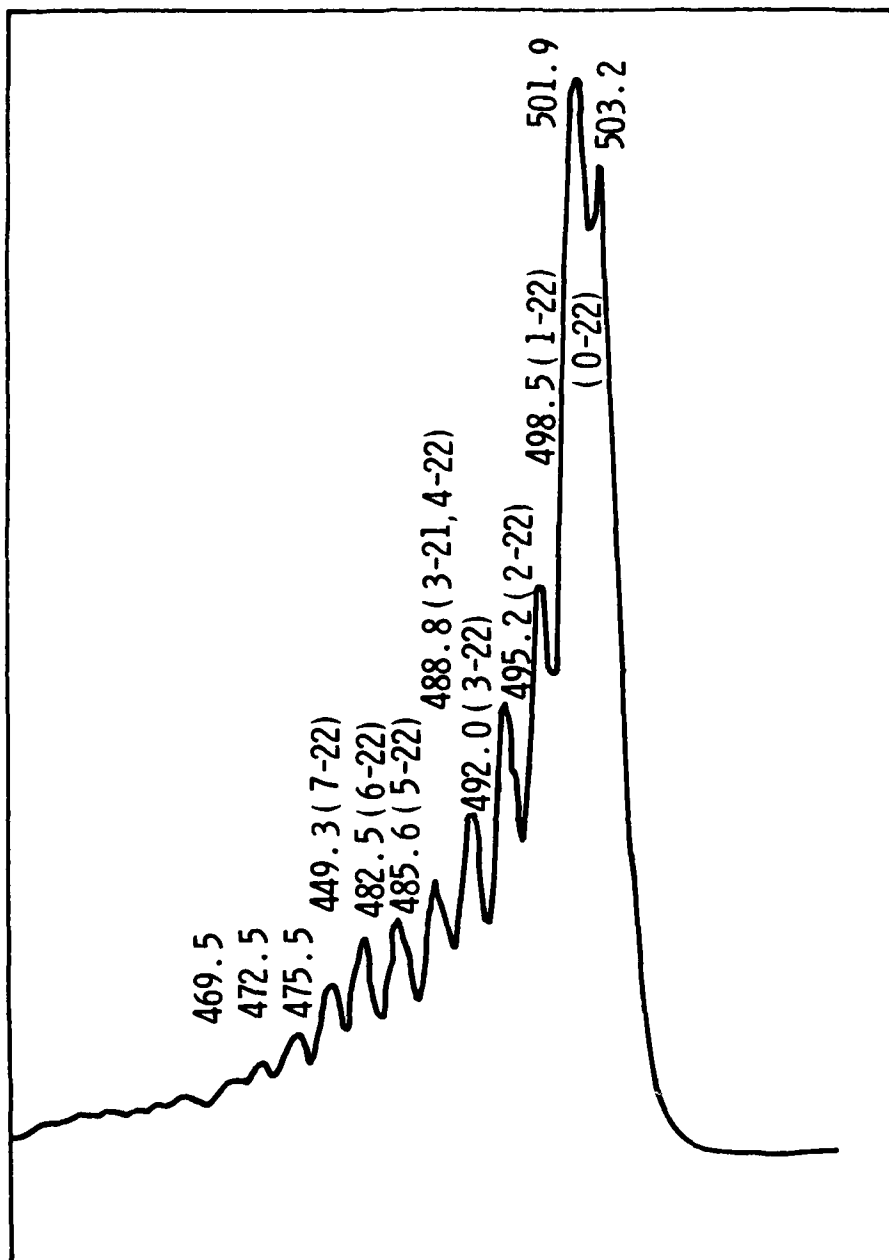
14

Fig. 7 — HgBr spectrum with 100 Torr N_2 and 900 Torr Ne buffer gas pressure fill at 300°K

The system lased with external mirrors of 100% and 80% reflectivity. The laser output was ~ 1 mJ at a charging voltage of 14 kV. The shapes of the laser pulse obtained at 12, 14, 16, 18, and 20 kV charging voltages are shown in Figure 8. The shapes were obtained with a fast photodiode. Replotting the data of Figure 8 similogarith-myically we obtain the curve shown in Figure 9 which yields a common decay time constant of 37 ns. Round trip time in the optical cavity was 8 nsec giving about 24 ns cavity decay time. An 18 nsec fluorescence lifetime[9] is consistent with the 37 nsec decay rate of the laser pulse. The integrated energy as a function of charging voltage is shown in Figure 10. The linear dependence is consistent with a constant glow voltage and the linear dependence of discharge current with charging voltage.

Recently Chang and Burhnam[12] have reported an increased efficiency of producing fluorescence in HgBr using Xe instead of N_2 as one of the buffer gas constituents. A mixture of 50 Torr Xe + 950 Torr Ne did not produce arc free glow discharges using the same circuit as above for charging voltages from 8 to 20 kV. A mixture of 50 Torr N_2 + 100 Torr Xe + 850 Torr Ne, however, did produce a diffuse discharge but the color of fluorescence is white instead of green at 120-150 °C cold spot temperature. Figure 11 shows a spectrum obtained using this mixture. Many lines are present and those at 528.7-541.9 nm coincide with known Xe spectra. The observed strong lines at 485.6, 488.8 and 492.0 nm match the fluorescence spectra of the HgBr discharge using N_2-N3 as a buffer shown in Figure 7. Xenon lines also overlap these lines to within 0.5 nm. Since the metastable level in Xe is about 2 eV above the HgBr upper laser level (B state) it is reasonable to expect that the transfer of energy from the Xe metastable to the HgBr system would leave the HgBr(B) in highly excited vibrational states or HgBr(C) state which then fluorescence down to the X state before reaching thermal equilibrium distribution with the buffer gas at the ambient temperature. If thermal equilibration were rapid we would expect the same spectra as shown in Figure 7.
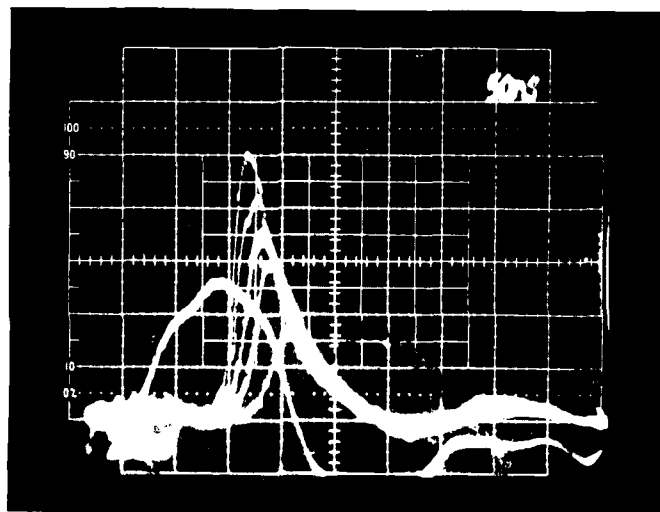
Fig. 8 – HgBr laser output pulse shapes for 12, 14, 16, 18, 20 kV
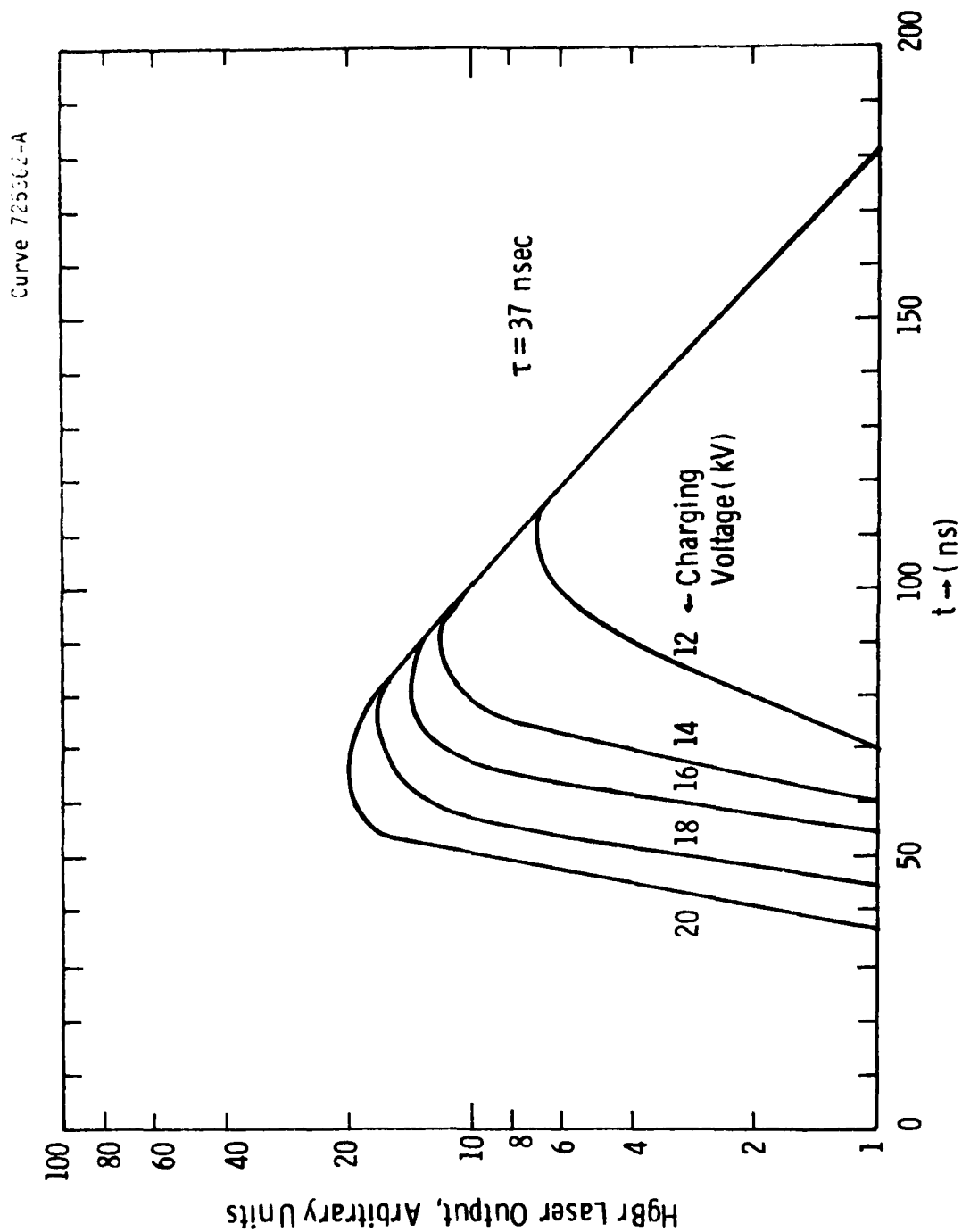charging voltage with discharge current at 20 kV.

17

Fig. 9 — Laser pulse at various capacitor charging voltages

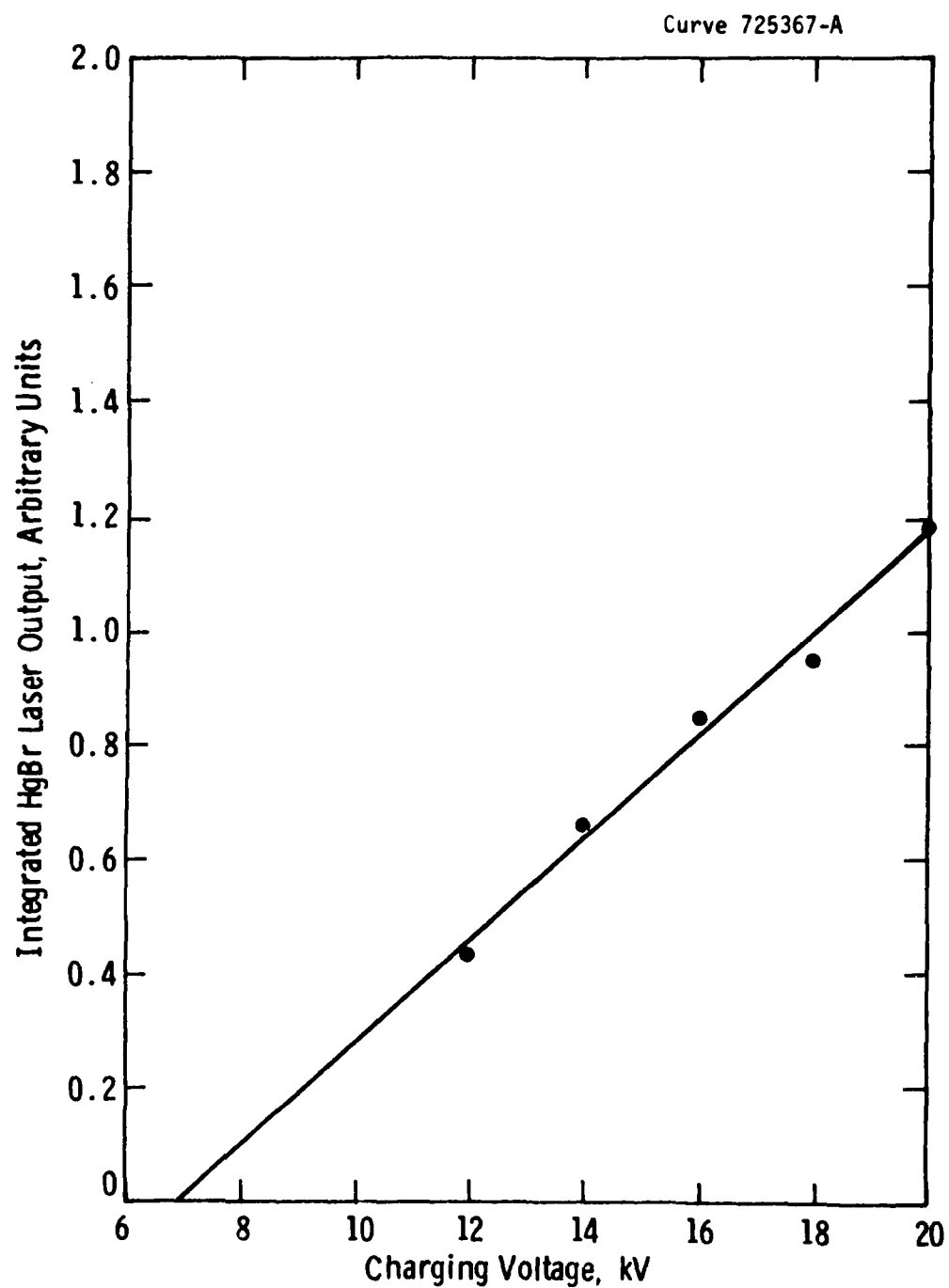Fig. 10 — Laser energy output as a function of charging voltage

546.1 (Hg)
541.9
537.2
533.4
528.7
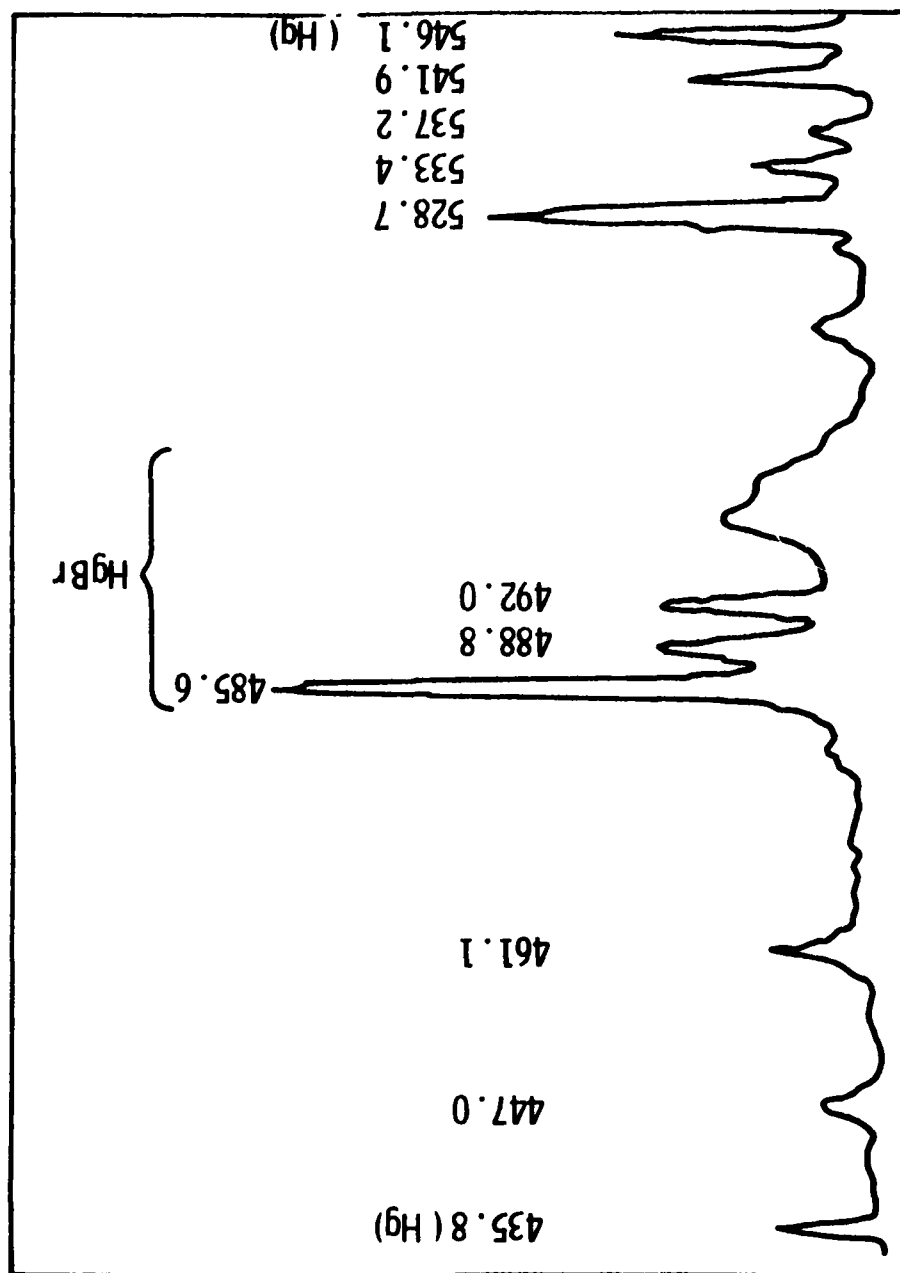
492.0
488.8
485.6

HgBr

461.1

447.0

435.8 (Hg)

Fig. 11 — HgBr spectrum using buffer gas fill of 50 Torr Xe + 100 Torr N_2 + 850 Torr of Ne at 300°K

CONCLUSION

We have achieved lasing in UV preionized self-sustained glow discharges of HgBr containing N_2 and Ne. Parameterization studies over a narrow range of conditions indicate that improved performance is likely to occur when additional changes in temperature, pressure, mixture, and power supply are made. To facilitate making these changes in a logical and relatively rapid manner, the apparatus will be shifted to an improved experimental test stand. These experiments will begin shortly. Meanwhile we report in this memo our preliminary encouragning results.

PERMANENT RECORD BOOK ENTRIES

Book #207983 - pp 121, 124-156
Book #208895 - pp 24-25, 48-81

This memo was typed by A. M. Tomasic.

REFERENCES

1. E. J. Schimitschek, J. E. Celto, and J. A. Trias, "Mercuric Bromide Photodissociation Laser", Appl. Phys. Lett., Vol. 31 (1 November 1977).

2. J. H. Parks, "Laser Action on the $B^2\Sigma^+_{1/2} \rightarrow X^2\Sigma^+_{1/2}$ Band of HgBr at 5018 Å", Appl.Phys. Lett., Vol. 31 (15 August 1977).

3. J. Gary Eden, "Green HgCl ($B^2\Sigma^+_{1/2} \rightarrow X^2\Sigma^+_{1/2}$) Laser", Appl. Phys. Lett. Vol. 31 (1 October 1977).

4. K. Y. Tang, R. O. Hunter, J. Oldenettel, C. Howton, D. Huestis, D. Eckstrom, B. Perry, and M. McCusker, "Electron-Beam-Controlled Discharge HgCl Laser", Appl. Phys. Lett., 32: 226 (15 February 1978).

5. W. T. Whitney, "Sustained Discharge Excitation of HgCl and HgBr $B^2\Sigma^+_{1/2} \rightarrow X^2\Sigma^+_{1/2}$ Lasers", Appl. Phys. Lett., 32: 239 (15 February 1978).

6. E. J. Schimitschek and J. E. Celto, "Mercuric Bromide Dissociation Laser in an Electric Discharge", Optics Lett., 2(3), (March 1978).

7. R. Burnham, "Discharge Pumped Mercuric Halide Dissociation Lasers", Appl. Phys. Lett., 33: 15 (July 1978).

8. E. J. Schimitschek and J. E. Celto, "Oscillator and Oscillator-amplifier Experiments with an $HgBr_2$/HgBr Dissociation Laser", Appl. Phys. Lett. 36 (3), p. 176 (1 February 1980).

9. Private communication.

10. R. C. Sze, "Rare-Gas Halide Avalanche Discharge Lasers", IEEE JQE, QE-15, No. 1, p. 1338 (December 1979).

11. Nai-Ho Cheung and T. A. Cool, "Frank-Condon Factors and r-Centroids for the $B^2\Sigma - X^2\Sigma$ Systems of HgCl, HgBr, and HgI", J. Quant. Spectra. Radiat. Transfer 21, p. 397 (1979.

12. R. S. F. Chang and R. Burnham, "Dissociative Excitation of $HgBr_2$ by Rare-gas Metastable Atoms and $N_2(A^3\Sigma^+_u)$", Appl. Phys. Lett., 36 (6), p. 397 (15 March 1980).

APPENDIX 2

VOLTAGE AND CURRENT MEASUREMENTS FOR FAST PULSED HIGH CURRENT DISCHARGES

J. L. Pack and I. Liberman
Westinghouse R&D Center
Pittsburgh, PA 15235

ABSTRACT

Some problems in obtaining accurate voltage and current waveforms of short pulse gas discharges are discussed. A method for correcting for the indudctance in the circuit is described which yields accurate discharge voltage and power input waveforms. A simple and economic current shunt having less than 5 ns rise time and negligible overshoot is described.

VOLTAGE AND CURRENT MEASUREMENTS FOR FAST PULSED HIGH CURRENT DISCHARGES

J. L. Pack and I. Liberman
Westinghouse R&D Center
Pittsburgh, PA   15235

I.   INTRODUCTION

Many laser systems, particularly excimers, require current pulses having rise times less than 50 ns and half widths of 100 ns or less.[1-5] Compact circuitry having minimum inductance is required to achieve these fast current pulses. Discharge voltage, current and power input waveforms are necessary for detailed analysis of laser system performance. This paper discusses some problems encountered in making these measurements. A simple analytical solution for a typical case and a method of deriving the discharge voltage from a measurement of the voltage applied to the terminals of the discharge tube are given. Also, a simple current shunt having less that 5 ns rise time and negligible overshoot is described.

II. LOW INDUCTANCE VOLTAGE AND CURRENT WAVEFORM ANALYSIS

Due to the inductance of leads, the measured voltage
waveform will always include some inductive component in addition
to the discharge voltage. For more compact, compacitance driven
discharge circuits, most of the circuit inductance is in the leads
within the discharge tube. Consequently, the voltage measured outside
the tube reflects the voltage on the capacitors rather than on the
discharge. A simplified diagram of a compact system used by Pack,
et al.[6] is shown in Figure 1. The discharge tube is closely coupled
to an LC inversion circuit,[2-9] preionizer circuit, high voltage
probe connection (V) and a 0.15 ohm current monitoring resistance
with a 91 ohm cable terminating resistance.

Waveforms obtained are shown in Figure 2. Here the
voltage waveform was obtained with the high voltage probe connected
to one of the feedthroughs to the pulsed anode of the discharge tube.
The cathode was connected to several feedthroughs (in parallel) to
a bank of 20-3 ohm-1 watt carbon composition resistors. This 0.15 ohm
resistance, rather than a Pearson current transformer, monitored the
discharge current and resulted in a compact low inductance system.
The inductance included in the portion of the circuit monitored by
the voltage probe was obtained by an analysis of the 2 waveforms.
When $dI/dt = 0$, the voltage drop across the included inductance, L_i,

is zero giving us the drop across the discharge, V_d, and the 0.15 ohm

series resistance, R. Assuming that the discharge did not arc; and

therefore, had a constant voltage at 10 ns before and after the time

$dI/dt = 0$, we can calculate L_i using the relation $V_m = V_d + L_i \, dI/dt + RI$

where V_m is the measured voltage. L_i was 200 nh consistent with the

size of the current loop in the experimental setup. Subtracting out

$L_i \, dI/dt$ from the measured voltage waveform, we obtain the calculated

voltage waveform which represents the voltage drop across the

discharge and the current monitoring resistance. The slight upward

curvature of the calculated voltage waveform reflects the 900 volt

drop across the 0.15 ohm resistance at current maximum.

For circuits containing more impedance such as capacitive

discharge circuits utilizing thyratrons[10] and cables[9] or PFN's to

couple energy into the discharge, the voltage waveforms may process

a characteristic more like that shown in Figure 3. The voltage

waveform tends to be linear[3-8,10] during the time, Δt, of current

flow. The discharge voltage, V_d, is obtained by noting the measured

voltage at maximum curre.. where $dI/dt = 0$. The reverse voltage

at current zero (t_2) gives us the included inductance, L_i, using

the relation $V_2 = L_i (dI/dt)_{t_2}$. Again, subtracting out Li dI/dt

from the measured waveform, we obtain the calculated discharge

voltage indicated by the dashed line in Figure 3.

III. DETERMINATION OF INPUT ENERGY

In addition to obtaining the discharge voltage, we wish
to determine the energy dissipated in the discharge. There are a
number of ways to obtain the energy from the voltage and current
waveforms. The most straightforward way is to perform a point by
point integration where the energy U is given by

$$U = \Sigma V_m \cdot I \cdot \Delta t$$

where the summation limits are from current zero to current zero.
A simpler, less tedious approach, is based on observing that for
these circuits the current is sinusoidal in shape, and that for
well behaved self-sustained discharges,[11] the discharge voltage is
nearly constant. Then the dissipated energy can be calculated as

$$U = \int_o^t V_d \cdot I_{max} \sin(\pi t / \Delta t)$$

$$= (2/\pi) V_d \cdot I_{max} \cdot \Delta t$$

where V_d is the discharge voltage which is equal to the measured
voltage at I_{max} (i.e., where $dI/dt = 0$).

For any method to work, it is important that the voltage and current traces be well synchronized. This usually means that the oscilloscope be triggered by the same signal for both traces, that the cables from the current and voltage probes have approximately equal length and that the probes themselves have negligible delay. Another important consideration is that the current probe is non-inductive so that the voltage measured will be proportional to I and not dI/dt.

IV. AN ECONOMICAL FAST HIGH CURRENT SHUNT

A bank of resistors was adequate to monitor the current in the above experiment but added losses to the system. For a low repetition rate application, this loss is not serious; however, for high repetition rate systems, this loss is undesirable. A lower resistance current monitor can be made in a number of ways. For high current fast pulses, Ekdahl[12] made an inductive current sensor for high z-pinch experiments. He achieved an inductance of 2 nh in his sensor and obtained the current by integrating his signal.

We have developed a purely resistive (in behavior) current monitor capable of handling multi-kiloampere pulses with ns resolution. This current shunt can be incorporated as a part of the discharge circuit so that no addition to the included inductance occurs.

By using a high resistivity metal, such as stainless steel or titanium to form part of the circuit, we obtain our built-in current monitor. For instance, a 2.5 cm wide 0.05 mm thick strip of stainless steel has 0.004 ohm resistance and about 4 nh inductance per cm of length. We return the current signal by means of a strip line to decouple this inductive component of impedance in the current shunt as shown in Figures 4a, 4b and 4c. Figures 4a and 4b show the construction of the resistive shunt tested. Using a Hewlett Packard 214 pulse generator as a source of a fast current pulse,

the 12.5 cm long strip gave a current sensitivity of 20 A/V, the

same as that of the Pearson current transformer and an output signal

which was a reproduction of the output pulse of the 214 with no

observable overshoot. This suggests a rise time of 5 ns or less

and that the inductive component of the signal was successfully

decoupled from the stainless steel strip by the action of the closely

coupled copper strip line. By folding it over as in Figure 4c, its

insertion inductance can be greatly reduced. A coaxial version of

this concept is described by Bak.[13]

V. SUMMARY

Inductive voltages in short pulse discharges and current monitors often exceed and mask the intended measurement of the resistive component of the voltage. By careful design, high current resistive current probes with a rise time of 5 ns or less can be made. Once an accurate current measurement is obtained, the discharge voltage and energy can be readily inferred from the measured voltage even though it contains a significant dI/dt component.

VI. ACKNOWLEDGMENT

This paper was typed by Debra Palmer.

VII. REFERENCES

1. J. L. Pack, C. S. Liu, D. W. Feldman and L. A. Weaver,
   Rev. Sci. Instrum., 48, 1047 (1977).

2. R. Burnham and N. Dseu, Appl. Phys. Lett., 29, 707 (1976).

3. R. C. Sze and P. B. Scott, Appl. Phys. Lett., 32, 479 (1978).
   and Rev. Sci. Instrum., 49, 772 (1978).

4. R. C. Sze and T. R. Loree, IEEE J. Quantum Electron. QE-14,
   944 (1978).

5. W. A. Fitzsimmons, L. W. Anderson, C. E. Riedhauser and
   J. M. Vrtilek, IEEE J. Quantum Electron. QE-12, 624 (1976).

6. J. L. Pack, D. W. Feldman, C. S. Liu and I. Liberman, Paper L. 4,
   International Conference on Lasers 1980, New Orleans, Louisiana,
   December 13-19, 1980, to be published in 1981.

7. A. J. Schwab and F. W. Hollinger, IEEE J. Quantum Electron. QE-12,
   183 (1976).

8. A. E. Greene and C. A. Brau, IEEE J. Quantum Electron. QE-14,
   951 (1980).

9. K. Matsumato, K. Sueoka, M. Obara, T. Fujioka and H. Yamamoto,
   Rev. Sci. Instrum., 51, 1046 (1980).

10. R. A. Olson, D. Grosjean, B. Sarka, Jr., A. Garscadden and P. Bletzinger, Rev. Sci. Instrum., 47, 677 (1976).

11. L. J. Denes and J. J.Lowke, Appl. Phys. Lett., 23, 130 (1973).

12. C. A. Ekdahl, Rev. Sci. Instrum. 51, 1645 (1980) and 1649 (1980).

13. C. K. Bak, Rev. Sci. Instrum., 48, 1227 (1977).

LIST OF FIGURES

Fig. 1 - Simplified circuit diagram.

Fig. 2 - Mercury bromide discharge characteristics.

Fig. 3 - Typical measured voltage and current waveforms.

Fig. 4 - Strip line current shunt.

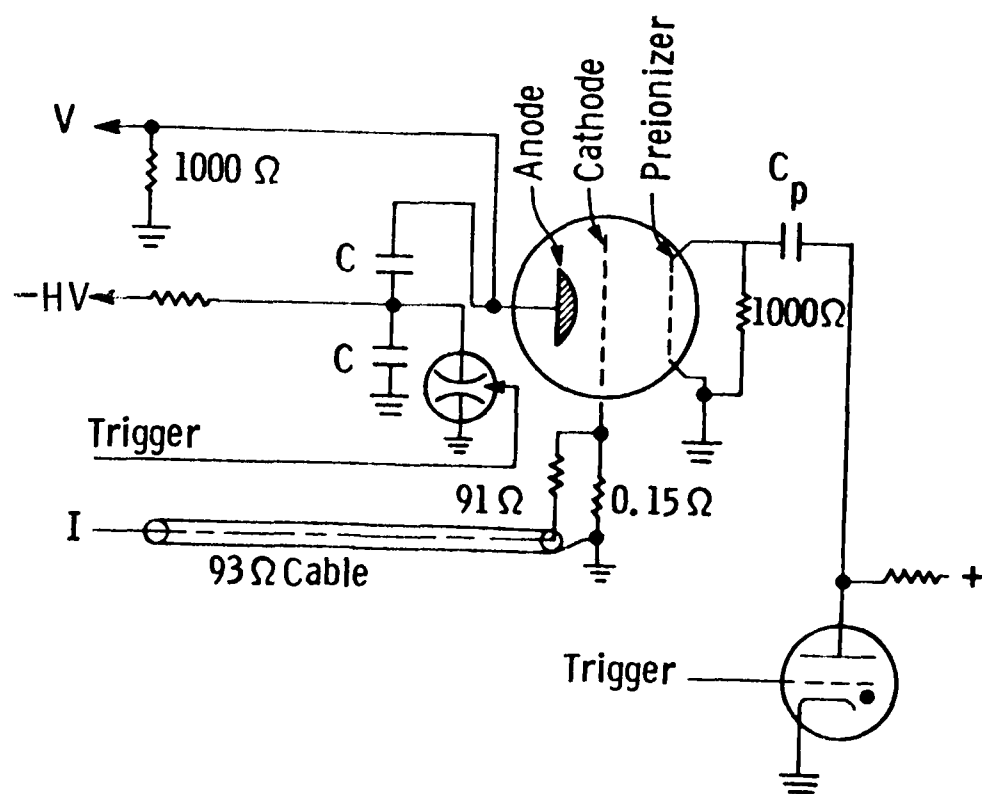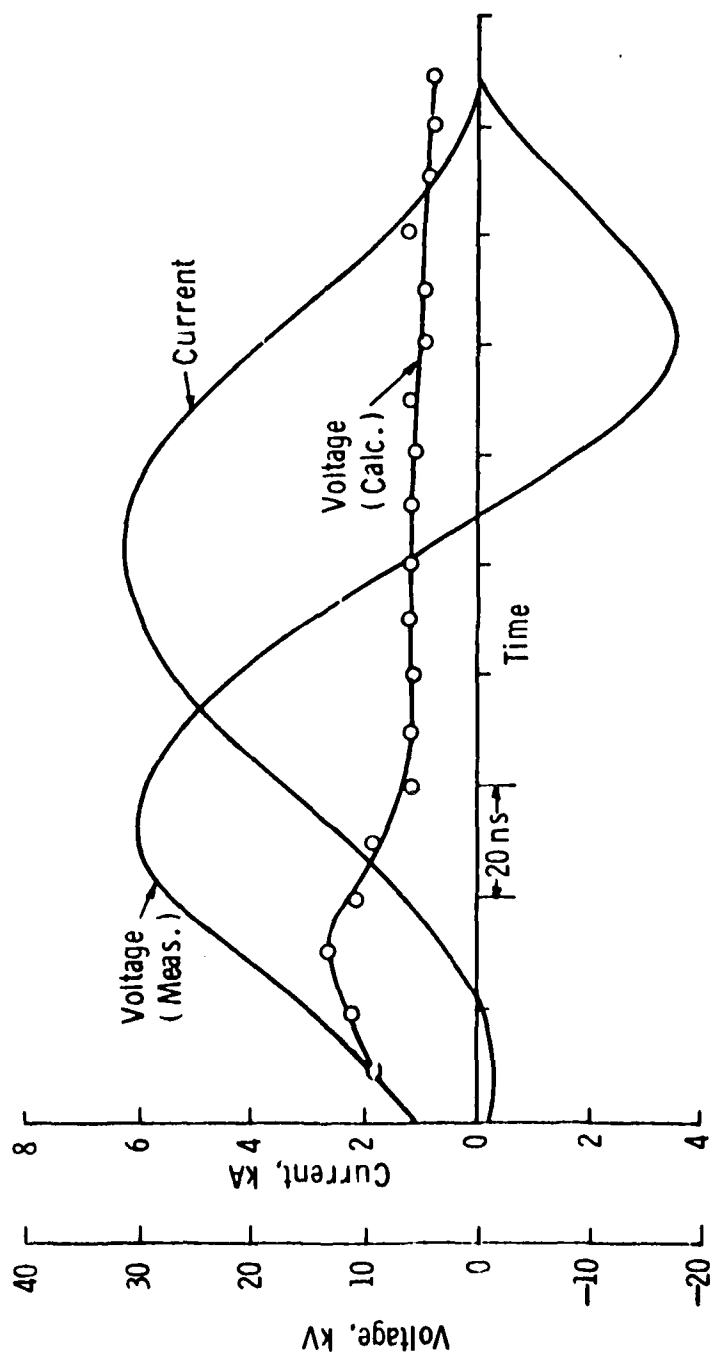Fig. 1 — Simplified circuit diagram

Curve 725605–A
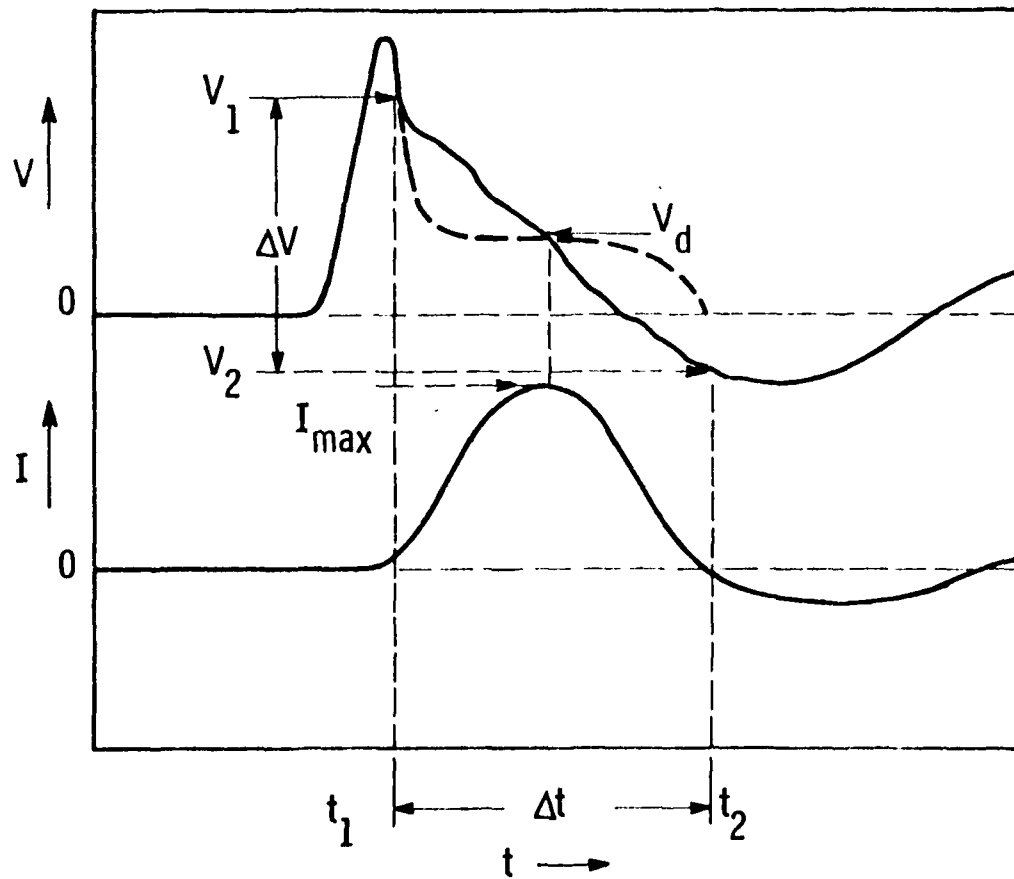
Fig. 2 — Mercury bromide discharge characteristics

Fig. 3 — Typical measured voltage and current waveforms